Interactions Between Halogens and the Simplest Carbonyls, Formaldehyde and Acetone

Timothy R. Corkish

Supervisor: Dr Duncan A. Wild

Honours Thesis submitted as part of the B.Sc. (Hons) degree

The School of Chemistry and Biochemistry

The University of Western Australia

Date of submission: 04/11/16

Declaration

I certify that the material of this thesis has not been submitted for any other award or degree at any institution.

To the best of my knowledge, any sources used in this thesis and any help received have been acknowledged within this thesis.

Tim Corkish, November 2016

Acknowledgments

Firstly, and foremostly, I would like to thank my supervisor Dr. Duncan Wild for all the guidance and teaching he has provided this year. This project has been a great experience and a large part of that is from everything I have learnt so far, and of course always being on the cusp of glory.

I would also like to give a big thanks to Peter Watson, who has been a great help in adjusting to the lab and was always more than happy to help out with anything I needed. Also to Damien t'Hart who has undergone this Honours year with me. It's been great to have someone to relate to and chat to as the year went on, and all your help was always appreciated. I'd like to give a mention to all the past members of the Wild group too, who have shaped this work with their own.

Lastly, I would like to thank my family for all their wonderful support as always, and to the West Coast Brawlers for keeping me sane throughout the year.

Abstract

Photoelectron spectra have been recorded for the chloride-acetone, bromide-acetone, and iodide-acetone complexes. Additionally, *ab initio* calculations were performed on the anion and neutral geometries of these clusters to complement and rationalise the experimental data. Calculations were also conducted of halide-formaldehyde clusters, with these results being used in a predictive sense. The rationale behind this study of complexes was to garner information related to the neutral potential energy surfaces, and in doing so, contribute to an understanding of atmospheric halogen interactions with simple carbonyl molecules.

Contents

List of Figures

1 Introduction

Investigating the properties of the interactions between halogens and the simplest carbonyls, acetone and formaldehyde, is the primary directive of this research. Within the context of atmospheric reactions, and through the use of a combination of mass spectrometry, photoelectron spectroscopy and computational studies, this project will aim to contribute to a greater understanding of the forces which govern and dictate the nature of halogen interactions with simple carbonyls. This chapter will set out the theory and background behind the techniques to be used and the motivations for studying halide-simple carbonyl clusters.

1.1 Atmospheric Chemistry

An interest in researching halogens and simple carbonyls stems from their relevance in an atmospheric environment. Halogens in particular have a well documented history of atmospheric activity, and are generally present in the troposphere and stratosphere as a result of volcanic eruptions, sea spray,[1] and anthropogenic emissions in the form of chlorofluorocarbons (CFCs). Stratospheric ozone destruction, catalysed by halogen species (most prominently chlorine) is now a well understood process,[2] and stands as perhaps the largest reason for interest in the study of the atmospheric halogen presence. The mechanism for this ozone destruction is shown in Equations 1.1, 1.2, and the net result in 1.3.[3]

$$\mathrm{X}^\bullet + \mathrm{O_3} \longrightarrow \mathrm{XO}^\bullet + \mathrm{O_2} \tag{1.1}$$

$$\underline{\mathrm{XO}^\bullet + \mathrm{O}^\bullet \longrightarrow \mathrm{X}^\bullet + \mathrm{O_2}} \tag{1.2}$$

$$\mathrm{O_3} + \mathrm{O}^\bullet \longrightarrow \mathrm{O_2} + \mathrm{O_2} \tag{1.3}$$

The catalytic destruction of ozone by the species X, where X may be a halogen radical or another such as the hydroxyl radical, highlights the importance of halogen interactions within an atmospheric context. In addition to their involvement in catalytic ozone destruction, halogens participate in a number of other atmospheric processes, and here attention is turned to those including simple carbonyls.

1.2 Halogens and Simple Carbonyls in the Atmosphere

Acetone has been described as the dominant non-methane organic species in the atmosphere with concentrations up to 2310 ppt measured over eastern Canada.[4] Sources generally include the oxidation of precursor hydrocarbons as well as some anthropogenic emissions in the form of biomass burning. The sinks of atmospheric acetone include degradation via photolysis and reactions with radicals (primarily the hydroxyl radical), which account for 64% and 24% of all atmospheric removal respectively. These sinks are of particular importance as the products of acetone degradation tend to result in the formation of peroxyacetylnitrates (PANs), which form a part of photochemical smog. Generally, acetone reacts with halogen radicals via a hydrogen abstraction, with an example shown in Equation 1.4. This example, a reaction between chlorine and acetone, highlights the importance of these interactions.

$$\mathrm{CH_3COCH_3} + \mathrm{Cl^\bullet} \longrightarrow \mathrm{CH_3COCH_2{}^\bullet} + \mathrm{HCl} \tag{1.4}$$

The hydrogen abstraction of acetone by the chlorine radical is by far the most dominant reaction pathway proceeding approximately 97% of the time,[5] with the competing addition pathway not entirely negligible. Computational studies have also shown that the reaction is favourable due to a small barrier height.[6] As mentioned previously, hydrogen abstraction via the OH radical is the most dominant radical reaction for acetone in the troposphere. However, in marine areas the impact of the OH radical is rivalled by the Cl radical.

The reaction between acetone and Cl has a reaction rate an entire order of magnitude higher than that of the OH reaction ((2.2 ± 0.4) x 10^{-12} cm^3 molecule^{-1} s^{-1} compared to (2.2 ± 0.5) x 10^{-13} cm^3 molecule^{-1} s^{-1}).[7] The implication of this is that in areas of higher chlorine concentration, such as within the marine boundary layer,[1] the hydrogen abstraction of acetone by the chlorine radical can dominate. As a result, halogen chemistry involving simple carbonyls can be at the forefront of atmospheric processes. That is not to say, however, that halogens other than chlorine are not relevant. Reactions involving fluorine and bromine do not contribute to the degradation of tropospheric acetone with the same impact as chlorine (although they proceed via the same hydrogen abstraction), but are important for theoretical purposes and as such these systems have garnered attention largely in the form of computational studies.[8,9]

Halogens react with formaldehyde via the same hydrogen abstraction channel as with acetone.[10] Also similarly, the major source of tropospheric formaldehyde is the oxidation of precursor hydrocarbons (namely methane) and the sinks include photolysis and reactions with radicals. The decomposition of formaldehyde is a large source for the formation of HO_x radicals, and so again the mechanisms of such decomposition are important to be aware of.

As in the case of chlorine and acetone, the reaction between the bromine radical and formaldehyde demonstrates the relevance of the atmospheric interactions between halogens and carbonyls. Bromine plays an important role in the loss of formaldehyde in the arctic troposphere, and the importance of this hydrogen abstraction is that it results in a reduction of the efficiency of bromine-catalysed ozone destruction.[11,12] Although this process is in the foreground with respect to the other halogens, the reactions between formaldehyde and fluorine,[13] chlorine,[13,14] and even iodine[15] have warranted experimental and theoretical studies. The work of Beukes et al.[13] is especially relevant to this project, with computational structures determined for the pre-reaction and post-reaction adducts as well as transition states for neutral halogen-formaldehyde reactions (the chlorine pre-reaction adduct structure is shown in Figure 1.1).

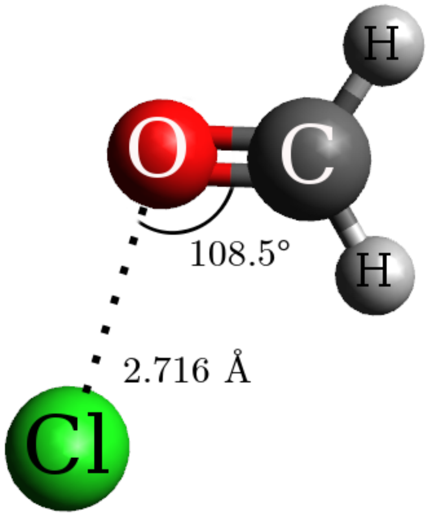

Figure 1.1: Cl + CH_2O pre-reaction adduct for the hydrogen abstraction reaction.[13]

A point of discussion has risen in the literature with Gruber-Stadler et al.[14] confirming the existence of the structure seen in Figure 1.1, yet finding it does not lie on the minimum energy path of the subsequent reaction. This is in favour of a pre-reaction adduct where the Cl atom resides along the CO axis. One aim of this project is to create gas-phase clusters resembling such important reaction points, coupled with calculations of geometries and energies, and in doing so make a contribution to this discussion through experiment.

1.3 Van der Waals Clusters

The courses of chemical reactions are typically difficult to map experimentally due to the unstable nature of pre-reaction and post-reaction adducts and of course transition structures. Studies such as those conducted in Figure 1.1[13] rely on computation to probe the nature of difficult or transient reaction species. However, some of these reaction states can be accessed through experimental means.

Demonstrable examples exist in the form of van der Waals clusters, weakly bound complexes between atoms or ions and molecules in the gas-phase.[16] 'Trapped' in a sense by their interaction for one another, these structures can resemble important points along a reaction pathway, such as pre-reaction adducts or transition states[17] and these structures can be studied experimentally. This project aims to use photoelectron spectroscopy and computational methods to investigate van der Waals clusters consisting of a halogen and either acetone or formaldehyde. In creating these gas-phase clusters and probing them via spectroscopy, the reaction dynamics between halogens and the carbonyls of interest can be examined, as well as the properties of the clusters formed.

1.4 Photoelectron Spectroscopy

One major aim of this project is to obtain photoelectron spectra of halide clusters with either acetone or formaldehyde in the gas-phase. First and foremost, photoelectron spectroscopy of ion complexes provides information about the neutral potential energy surface (PES).[18] A PES is the relation of a system's potential energy with respect to the position of the nuclei. That is to say, information about the structure and energetics of the neutral species can be derived. Hence, the previously mentioned atmospheric reactions involving halogens, acetone, and formaldehyde can be investigated using ion-molecule spectroscopy through probing the structure of the neutral-neutral reaction species.

Another property that can be examined using ion-molecule spectroscopy is the nature of ion solvation.[19] As with transient reaction species, the nature of ion-molecule (solute-solvent) interactions is difficult to ascertain through experimental measurements of the solution. Instead, ion-molecule spectroscopy can be used to study the structure of ion-solvent bonds, electronic and vibrational states, and indeed the positioning of the species in relation to one another. While ion-molecule solvation is not the primary concern of this project, it is necessary to keep in mind pending experimental observations. Previous research in the Wild group has focused centrally upon the nature of ion-molecule solvation.[20]

1.4.1 Anion Photoelectron Spectroscopy

Anion photoelectron spectroscopy is a derivative technique based on the photoelectric effect and will be used throughout this project to investigate gas-phase halide clusters with either acetone or formaldehyde. It was previously stated that ion-molecule spectroscopy can be used to probe the PES of a neutral species. This is achieved through photodetaching an electron from the anion species AB^- to form the neutral AB. The kinetic energy of the photodetached electron (ϵ_{KE}) corresponds to the binding energy of the system (ϵ_{BE}) as follows:

$$\epsilon_{KE} = h\nu - \epsilon_{BE} \tag{1.5}$$

Knowledge of $h\nu$, the energy of the input photon (generally UV), and measurement of the energy of the photodetached electrons allows for the binding energy of the system to be determined. This corresponds to the electron affinity (or in other words, the difference in energy between the anion cluster and neutral cluster) of the neutral species.[21] One of the first uses of this technique was to determine the electron affinity of the helium atom ($He^{-} \longrightarrow He$).[22] As seen in Figure 1.2, the variation in energies of the emitted electrons correspond to different vibrational transitions. As a result, photoelectron spectroscopy can be used to investigate the vibrational structure of a system, provided the experimental resolution is high enough.

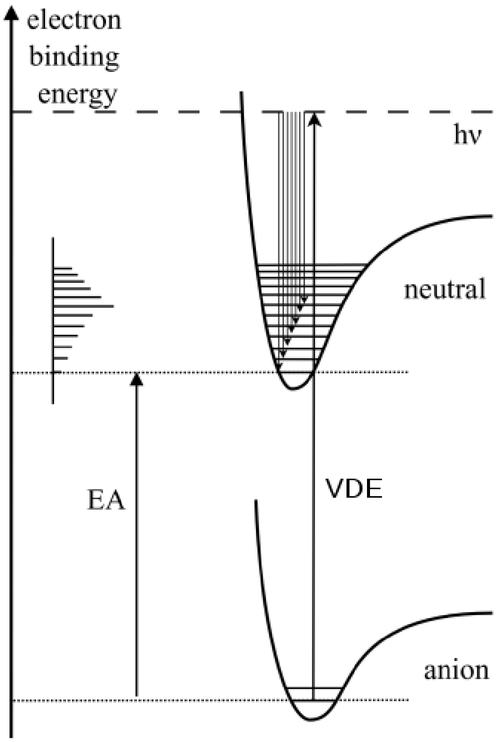

Figure 1.2: The main process behind photoelectron spectroscopy. The potential energy surfaces of the anion and neutral species are shown.[23]

Other parameters that have been drawn from experiment include gas-phase acidities, ionisation energies, and bond dissociation energies.[24] Relevant to this project are the extraction of the adiabatic energy EA, pictured in Figure 1.2 as the 0 to 0 (or ground-state to ground-state) transition, and the vertical detachment energy (VDE), in addition to the complex dissociation energies D_0. The VDE is the most likely or favourable transition as according to the Franck-Condon principle, and should be shown spectroscopically as the most intense peak.

The Franck-Condon principle states that the mostly likely transition is one that results in a minimal change in geometry, as the movement of electrons is almost instantaneous relative to the larger nuclei. Reflecting the ground-state to ground-state transition, the EA should correspond to the highest electron ϵ_{KE} observed. Both the EA and VDE are facets of the overall binding energy of the system.

1.4.2 Previous Research on Complexes

Examples of notable work in the field of photoelectron spectroscopy have come from the groups of Lineberger,[25] Neumark,[26] and Wang.[27] Additionally, research by Markovich[28,29] has led to insights into the solvation behaviour of halide-H_2O complexes. Neumark's account of photoelectron spectroscopy experiments displays how such experiments can be used to probe the PES of a neutral-neutral reaction.[30] So far, there has been no research conducted on the photoelectron spectra of halide-acetone or halide-formaldehyde complexes. Therefore, the features of this work will be novel and will add knowledge to this area.

The Wild group has had previous success in taking photoelectron spectra of halide-acetylene,[31] halide-nitrogen,[32] and halide-carbon monoxide[33–35] complexes. Of particular interest to this project are the results of the halide-carbon monoxide studies, given that formaldehyde and acetone are related closely in structure. An *ab initio* study of the $Ar \cdots CH_2O$ complex noted this assumption, stating that the results gathered for the system were 'strikingly similar' to that of $Ar \cdots CO$.[36]

Research on the $Cl^- \cdots CO$ complex found a complex binding energy of 14.6 kJ mol^{-1} and a stabilisation energy (difference in energy between the photoelectron peak of the bare Cl^- ion and the corresponding peak of the complex) of 0.16 eV.[33] The work of this project will seek to compare with these results with the chloride-acetone and chloride-formaldehyde spectra (in addition to the other bromide and iodide complexes) and make rationalisations as to the reasons for any differences.

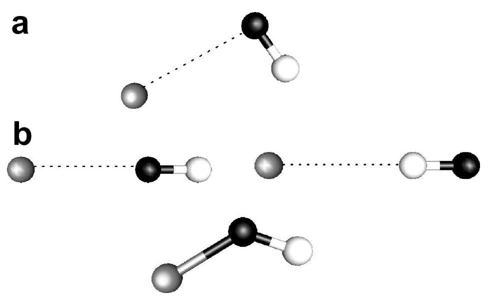

Figure 1.3: Computer structures of (a) $Cl^{-}\cdots CO$ anion, and (b) $Cl\cdots CO$, $Cl\cdots OC$ and ClCO neutral van der Waals clusters.[33]

Figure 1.3 shows the computed structures of both the anion complex (a) and the neutral complex as well as ClCO (b). Throughout this project these structures will be useful for both structure elucidation of the corresponding acetone and formaldehyde clusters and for comparative discussion.

1.5 Computational Theory

Computational chemistry is a tool used to provide theoretical data, and the techniques involved have been developed to an extent that this data can be used in a predictive sense. In exploring the PES of a molecule, features such as bond lengths and angles, energies, and even spectra can be calculated for normally difficult systems to study experimentally.[37] In addition to photoelectron spectroscopy, this project will make use of *ab initio* calculations to probe the clusters of interest, inciting interplay between the experimental and theoretical results.

Ab initio calculations describe a method of computation without any experimental input, or in other words, from first principles. These calculations provide solutions to the many-body, time-independent Schrödinger Equation (1.6) based upon the Born-Oppenheimer Approximation. This approximation is fundamental in determining solutions to the electronic structure problem, and describes how the motion of nuclei and electrons can be treated as separate. $\hat{H}$ is the Hamiltonian operator consisting of kinetic and potential energy operators, and acts upon the wavefunction Ψ to produce energy eigenvalues (E). As a result, quantised energies of a system can be determined.

$$\hat{H}\Psi = E\Psi \tag{1.6}$$

The calculations conducted in this project are based on *ab initio* methods including Hartree-Fock (HF), second order Møller-Plesset Perturbation Theory (MP2), and coupled cluster theory with excited singlets, doublets, and perturbative inclusion of triplets (CCSD(T)). The HF method is one of the earliest computational models used to solve the Schrödinger equation for a multi-electron system. Essentially, these multi-electron systems become difficult to approximate due to the effects of interaction between each electron. The HF method deals with this problem by approximating an average field of electron interaction.[38] However, one problem of the HF method is that the treatment of electron interaction as a consistent field does not take into account electron correlation energy (electron repulsion). A number of subsequent *ab initio* methods, known collectively as post-HF methods, were developed to combat this.

MP2 calculations have been shown to account for up to (92.4±4.6)% of the total electron correlation energy.[39] The perturbation theory treats the Hamiltonian operator as two parts: an unperturbed Hamiltonian and a perturbation.[40] MP2 calculations have traditionally shown consistent results however one disadvantage is that the second-order energy correction results in a lowered ground state energy.[20] Another disadvantage of MP2 theory is that higher basis sets are required for more accurate results.[39]

CCSD(T) is another post-HF method and makes use of excitation operators (i.e. the virtual excitation of electrons) in accounting for electron correlation energy.[37] Importantly, the effect of excited triplet states is only approximated to save on computational expense. CCSD(T) calculations are known to yield highly accurate results, with the use of CCSD(T) compared to CCSD with the same basis set reducing error by up to an order of magnitude.[41] The calculations conducted in this work will approach this level of theory and the results will be used to complement experimental data.

1.6 Project Aims

The aims of this project can be formalised as follows:

1. To create gas-phase anion clusters consisting of a halide (Cl^-, Br^-, I^-) and either formaldehyde or acetone.
2. Use a combination of mass spectrometry and photoelectron spectroscopy to probe the structure and properties of these clusters (such as the EA and VDE).
3. Use computational chemistry to rationalise and complement the experimental results.

Anion photoelectron spectroscopy of halide-acetone and halide-formaldehyde clusters will garner information related to the neutral states of these complexes. Specifically, the spectra will allow parameters such as the adiabatic energy EA (also referred to as the electron affinity or complex binding energy), vertical detachment energy VDE, and the stabilisation energy to be extracted. Determining optimised structures through computation for both the anion and neutral species will provide structural information of the clusters, and the calculated energies will be able to predict features such as the binding energies (EA and VDE) of the system and dissociation energy D_0. As such, the computational and experimental results will complement each other and allow for greater insight into these clusters.

The significance of this project lies in taking photoelectron spectra of halide-acetone and halide-formaldehyde clusters, something which as not yet been achieved. In making comparisons to previous research[33–35] and drawing on points of discussion within the current literature,[13,14] this work will seek to add to a greater understanding of the nature of halogen interactions with simple carbonyls.

2 Materials and Methods

This section will provide an overview of the techniques used in experiments. The preparation of gas mixtures, workings of the time-of-flight photoelectron spectrometer (TOF-PES), and spectral data analysis will be explained. Additionally, the specific computational methods will be rationalised in terms of separate data analyses. Any modifications to conventional methodology and troubleshooting strategies will be detailed throughout this section.

2.1 Gas Mixture Creation

The first point of experimentation was the creation of the gas-phase anion clusters. A halide donor species (CCl_4, CH_2Br_2, and CH_3I), the solvating species (acetone) and argon were brought together in a gax mixing chamber in a ratio of approximately 1:9:90. The argon acts as a buffer gas and also provides vibrational cooling of the nascent clusters.

Before a new gas mixture could be introduced into the chamber, the previous mixture was evacuated. A rotary pump combined with a liquid nitrogen trap, to improve efficiency, was used to remove the previous gas mixture. At least three pumping cycles to approximately 20-30 mTorr took place, with each evacuation accompanied by an argon flush of the chamber in an attempt to incite as much desorption from the inner surfaces as possible. The argon was introduced via a gas bottle whereas the halide sources and solvating species, being liquids, were brought in via two attached flasks using their vapour pressures.

A freeze-pump-thaw method was used to degas the liquid samples. This involved freezing the sample in a liquid nitrogen dewar, evacuating over the top of it with a vacuum line, closing off the vacuum, and thawing the sample out. Each liquid species was then opened to the gas mixing chamber and allowed to enter as a result of their vapour pressure. One problem encountered was that in separate cases too much halide source, or too much acetone, was introduced into the mixing chamber. This resulted in a greater abundance of halide-halide donor clusters (i.e. $I^{-}\cdots CH_3I$) being produced and making it difficult to study the cluster of interest. In the case of acetone, excess amounts in the chamber led to the formation of unstable clusters, believed to be the result of condensation at the opening of the nozzle apparatus. To better control the amount of the sample allowed into the chamber, ice-water (for the halide-donor species) and dry ice-acetone (for acetone) baths were used to lower the temperature of the species and subsequently its vapour pressure upon introduction to the gas mixing chamber.

Purified acetone was also used to minimise the instability in acetone cluster production by reducing the amount of contamination. This worked to moderate success although the problem was not entirely accounted for. Unfortunately, due to time constraints as well as technical issues, no halide-formaldehyde mixtures were able to be made.

After the halide source and solvating species were introduced into the mixing chamber, having rested for several minutes each, the mixture was made up to approximately 450 kPa using argon. The mixture was then left to mix for at least a day, with some clusters needing more time for the equilibration of the mixture, as seen through the ion signal increasing during experimentation.

2.2 Overview of the TOF-PES

A time-of-flight mass spectrometer coupled to a photoelectron spectrometer (TOF-PES) was used to record mass and photoelectron spectra throughout experimentation. The TOF-PES is based on a Wiley-McLaren[42] style mass spectrometer, and was constructed by LaMacchia[43] during his Honours year. Figure 2.1 shows a top-down view of the TOF-PES, detailing the source chamber, where the gas mixture is initially injected and anion clusters formed, and the extraction chamber, where negatively charged ions are sent down the time-of-flight axis (right to left on the diagram). The ions then drift towards either the ion detection chamber (for mass spectrometry experiments) or are intersected by a laser pulse in the laser interaction chamber (used in photoelectron spectroscopy experiments).

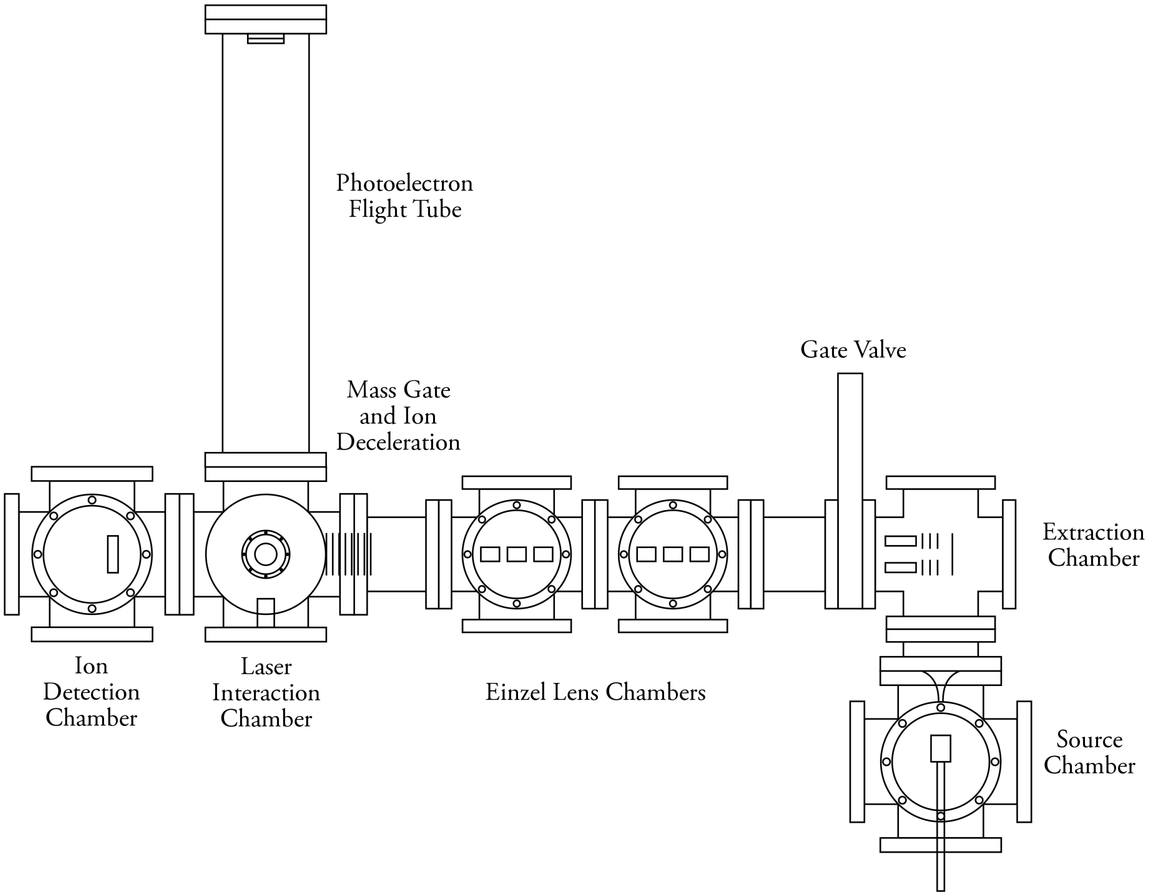

Figure 2.1: Top-down view of the TOF-PES apparatus.

The mass spectrometer allows the selection of ions or clusters down the time-of-flight axis based on their mass. As the same time-of-flight mechanism is used during the recording of photoelectron spectra, the clusters of choice can be honed in on prior to the detachment of photoelectrons. Sections 2.2.1 and 2.2.2 will detail the inner workings of the apparatus during both mass spectrometry and photoelectron experiments, before 2.2.3 will elaborate on the laser interaction procedure during the photoelectron experiments.

2.2.1 Cluster Formation and the Source Chamber

The source and extraction chambers are kept at a resting vacuum of 1 x 10^{-8} Torr through the use of two diffusion pumps backed by a rotary pump, with this pressure rising to mid 10^{-5} values during experiments. One problem encountered during this project was that the low vacuum was not being achieved easily, suggesting that the diffusion pump attached to the source chamber was not running efficiently. The pump was removed from the machine, thoroughly cleaned, and the oil inside vacuum distilled to purify it. The inherent problem, however, was that the heating pad underneath the pump was not in proper contact with the pump itself. Additionally, the smaller heating element was not operational and needed replacing. This meant the oil inside was not being heated or subsequently vapourised efficiently, leading to a reduction in how low a vacuum could be achieved. Once this was fixed, low vacuum environments were once again possible.

The gas mixture is pulsed into the source chamber via a solenoid nozzle and undergoes a supersonic expansion as it does so. This gas expansion is intersected by a pulse of electrons from a rhenium filament. The current emitted from the filament as well as the timing and width of a pulsed bias can be controlled externally, allowing the conditions of electron bombardment to be optimised.

Additionally, an Einzel lens is positioned next to the rhenium filament. This Einzel lens allows the emitted electrons to be focused to a central point in the gas expansion, meaning that the position of maximum intersection and thus cluster formation can be controlled. Through a process of dissociative electron attachment (Equations 2.1-2.3), as opposed to direct electron ionisation, the negative ions and clusters are formed.

$$\mathrm{Ar} + e^-_{fast} \longrightarrow \mathrm{Ar}^+ + e^-_{slow} + e^-_{fast} \tag{2.1}$$

$$e^-_{slow} + \mathrm{CH_3I} \longrightarrow [\mathrm{CH_3I^-}]^* \longrightarrow \mathrm{CH_3} + \mathrm{I^-} \tag{2.2}$$

$$\mathrm{I^-} + \mathrm{C_3H_6O} \longrightarrow \mathrm{I^-} \cdot\cdot\cdot \mathrm{C_3H_6O} \tag{2.3}$$

A plasma containing the anion species of interest, as well as neutrals and cations, is formed. Optimising the electron filament conditions to produce cluster species for experimentation is often one of the most crucial steps. The formation of acetone clusters was generally more favourable with a higher filament current, especially prior to using a dry ice-acetone bath to reduce the proportion of acetone in the gas mixture. The higher filament current may have led to a temperature increase that aided in removing any condensation on the tip of the nozzle. As a note, future work on the TOF-PES will involve a replacement of the solenoid nozzle with a Piezo nozzle, with the goal being to improve the reproducibility of each nozzle pulse.

A small central portion of the plasma passes through the skimmer into the extraction chamber. Here, the anions and anion clusters are separated from any other species in the mixture and are sent down the time-of-flight axis.

2.2.2 Ion Extraction and Flight Tube

Once the plasma arrives into the extraction chamber via the conical skimmer, a series of TOF plates send the negatively charged species down the time-of-flight axis. The TOF plates consist of two negatively charged plates and one grounded plate. When the plasma passes by the TOF plates, the anion species are repelled down the time-of-flight tube, with cations sent the opposite way and the neutrals largely unaffected. As one of the plates has a larger negative voltage applied to it (generally -910 V for one plate and -1000 V for the other) any anions or anion clusters that have drifted as a result of the gas expansion are literally brought up to speed.

Towards the latter end of this project the voltages of the two TOF plates were brought to -1350 V and -1500 V respectively. The quality of the ion signal observed was low when using the previous -910 V/-1000 V settings. This suggested that the nozzle pulse or gas expansion was offset in some way, with the anions requiring more energy to be sent down the flight tube with the required trajectory. An interesting point to note was that when the charges on the plates were reversed, with the front plate now at -1500 V and the back at -1350 V, ion signals were mostly unaffected. It would be expected that the orientation of the charges would repel the negative ions in the opposite direction to the flight tube and no signal would be observed. This suggested that the beam was offset in such a way that it was clipping one of the TOF plates. Although ion signal is easily observable troubleshooting this issue is still ongoing.

As the anion species leave the extraction chamber, they are steered with a set of charged X-Y deflection lenses. Due to Coulombic repulsion, the beam of anions and negatively charged clusters separate as they head down the time-of-flight tube. A set of two Einzel lenses are used to reduce this problem. Another addition to the TOF-PES apparatus was a second set of X-Y deflection lenses midway through the flight tube to further the steering of the ions. These second X-Y plates were able to improve the ion signal quite well, suggesting that even after beam correction with the first set of X-Y plates as well as the Einzel lenses that the beam was slightly offset or passing through the flight tube on an angle.

It is in the flight tube where the negative ions are separated according to their mass, as they all have the same approximate kinetic energy. Mass spectra can be recorded with the ions reaching an ion detector at the end of the time-of-flight tube. Conditions such as the timing of the TOF plate pulse with respect to the gas nozzle pulse, charges on both sets of X-Y deflection plates, and the potential applied to the Einzel lenses are optimised to provide the greatest signal of ions resulting from the flight of their path. The cluster of interest can then be interesected with a laser for photoelectron spectroscopy experiments.

2.2.3 Laser Interaction

In the photoelectron experiments a pulse of UV radiation at 266 nm (the quadrupled output of a Nd:YAG laser corresponding to 4.661 eV) coincides with the arrival of the desired anion cluster in the laser interaction chamber. This radiation has sufficient energy to eject an electron from the cluster, forming the neutral complex in the process. The ejected electrons are directed towards the photoelectron detector through the use of a bottleneck-shaped magnetic field.[20] The purpose of the shape of this magnetic field is to capture as many photoelectrons as possible.

The laser optics were typically optimised to provide a low intensity output. A high laser power would result in many more photoelectrons being captured at the cost of a notably increased amount of noise, with the laser ejecting electrons from apparatus within the TOF-PES due to the photoelectric effect. The unwanted electrons are directed down to the detector and add to an increased amount of background noise observed. Additionally, a heightened noise level makes it difficult to identify the point of laser intersection with the cluster of interest.

All experiments are pulsed at 10 Hz, with the spectra collected the result of up to ten thousand pulses. The timing and intensity of the optimisable parameters mentioned in this section, such as the TOF plates and X-Y deflection plates, are presented in a schematic in Appendix B. Finding the best arrangement to provide the greatest conditions of cluster formation and flight path is of high importance for photoelectron experiments.

2.3 Experimental Data Analysis

2.3.1 Mass Spectra

Mass spectra were recorded using an oscilloscope (Agilent, DSO6034A, 300 MHz) coupled to the TOF-PES to average the time-of-flights of all ion species. The averaging process typically took place over 256 pulses of the nozzle with the spectra subsequently saved to a computer. Following on, the mass spectrum could be calibrated, i.e. conversion of the x-axis from time-of-flight to m/z. The bare halides were easily distinguishable through large signals and unique splitting patterns. Assigning mass values to these peaks on the computer allowed for a calibration curve to be determined (using ^{79}Br^{-}, ^{81}Br^{-}, and ^{127}I^{-}).

From this, the m/z ratios of other clusters could be determined, allowing for the clusters of interest to be pinpointed. Following the calibration of the mass spectra, the peaks of interest could be optimised to provide the best signal for photoelectron experiments.

2.3.2 Photoelectron Spectra

The photoelectron spectra were recorded with each photoelectron arriving at the detector counted as a distinct event. The number of these events are recorded along a series of time bins using an ultra fast time-of-flight analyser (FastComtec, P7888, 2 ns resolution). In terms of the raw data, this corresponds to the number of photoelectrons captured by the detector as a function of their time-of-flight (or kinetic energies). A typical data set will include three spectra of the cluster of interest (for averaging) as well as a spectrum of the bare halide (for calibration and determination of E_{stab}) and a background. The first step of data analysis is a conversion of bin number to time-of-flight using Equation 2.4.

$$TOF = ((16(fstchan)) + 2(bin - 1)) \times 10^{-9} \tag{2.4}$$

$fstchan$ corresponds to the start delay (taken from the .888 file and is usually 0), and bin is simply the time bin number. Viewing the spectrum of the bare halide (now photoelectron counts as a function of time-of-flight) allows the $^2P_{3/2}$ and $^2P_{1/2}$ peak positions to be determined in terms of time-of-flight. A plot of the known kinetic energies of these halide peak positions at 266 nm (shown in Table 2.1 and derived from known binding energies (from NIST)[44] and the 4.661 eV input photon as per Equation 2.6) against $1/TOF^2$ results in a linear function of the form shown in Equation 2.5.

$$\epsilon_{KE} = m(\frac{1}{TOF^2}) + c \tag{2.5}$$

$$\epsilon_{KE} = h\nu - \epsilon_{BE} \tag{2.6}$$

Table 2.1: Known kinetic energies of the bare halides using a 266 nm input photon.

Halide peak	Known ϵ_{KE} at 266 nm (eV)
Bromide $^2P_{3/2}$	1.2974
Bromide $^2P_{1/2}$	0.8405
Iodide $^2P_{3/2}$	1.6020
Iodide $^2P_{1/2}$	0.6593

Through a linear regression analysis the values of c and m in Equation 2.5 can be determined. As a note, the calibration for the $Cl^{-}\cdots$acetone spectra was conducted using the closest day where a base I^{-} spectrum was taken due to the splitting of the Cl^{-} $^2P_{3/2}$ and $^2P_{1/2}$ being less than the resolution of the apparatus, making the determination of the individual peak positions difficult. The time bins are now converted to time-of-flight, and time-of-flight can then be converted to ϵ_{KE} using the fitted Equation 2.5. Equation 2.6 then allows ϵ_{BE} to be calculated based on the 4.661 eV input photon. Photoelectron spectra are presented as a function of ϵ_{BE} as opposed to ϵ_{KE} due to different input energies ($h\nu$) used by different experimenters.

The photoelectron counts of the three cluster spectra are averaged, smoothed, and the background count subtracted. As a final step a Jacobi transform is applied, which involved multiplying the intensities by TOF^3. This transformation is needed as the conversion from TOF to ϵ_{KE} is not linear, and hence the intensities which are originally expressed in time bins, need to be converted to energy bins. A plot of the new intensities as a function of ϵ_{BE} can now be constructed and the binding energies can then be determined for the cluster upon inspection of the spectra over the range of 0 to 4.661 eV. E_{stab} is then the difference between the peak positions of the bare halide and those of the cluster in eV.

2.4 Computational Methods

Calculations on the halide-formaldehyde and halide-acetone anion and neutral clusters were performed using a combination of the Gaussian 09[45] and CFOUR[46] programs. The level of theory of geometry optimisations approached the CCSD(T) level following initial MP2 computation, with Dunnings[47–52] correlated consistent basis sets up to quintuple zeta (aug-cc-pVXZ where X = D, T, Q, 5). A suite of geometry optimisations were conducted initially at the MP2/aug-cc-pVDZ (pVDZ PP for iodide) level to determine potential minima along the PES of the complex of interest. Following this, calculations were perfomed at the MP2/aug-cc-pVTZ (aug-cc-PV(T+d)Z level for Cl and aug-cc-pVTZ PP for Br and I) level. The custom basis sets not included in the programs were downloaded from the EMSL Basis Set Exchange,[53] with these basis sets providing more accurate energies for the chlorine systems or in the case of Br and I, freezing the energies of core electrons to save on computational expense.

Upon successful geometry optimisations, frequency analyses were performed to determine whether the geometry was a true minimum (all real frequencies), a transition state (one imaginary frequency), or a higher order saddle point (more than one imaginary frequency). Subsequent single point energies were determined at the aug-cc-pVQZ and aug-cc-pV5Z levels in order to perform a complete basis set (CBS) extrapolation to arrive at more accurate total energies, which will be explained in further detail in the next section on data analysis.

The convergence of the same geometries at the CCSD(T)/aug-cc-pVTZ (and related custom basis sets) level proved to be somewhat difficult in Gaussian 09, due to the procedure using numerically determined gradients in combination with the shallow potential energy surfaces of the investigated complexes, meaning that a minimum point was difficult to converge to. Some troubleshooting methods involved reducing the step size of each optimisation (thereby limiting how much the geometry is allowed to change at a position close to the minima) and accompanying the optimisation input files with a frequency output from a lower level of theory (in order to direct the optimisation towards a known minimum), but these proved unsuccessful.

The greatest improvement in converging CCSD(T)/aug-cc-pVTZ geometries came upon switching to the CFOUR program, using a different algorithm in calculation which evaluated gradients analytically rather than numerically. Additionally, constraining key symmetry elements (such as dihedral angles in a C_s structure to 180.0°) aided the optimisation process. This technique yielded success in optimising all halide-formaldehyde anion structures as well as the oxygen-appended neutral geometries described by Beukes et al.[13]

Single point energy calculations on the CCSD(T) optimised structures up to quintuple zeta were conducted to provide highly accurate data for the CBS extrapolation. These energy calculations do not separate the $^2P_{3/2}$ and $^2P_{1/2}$ energies from one another, so during data analysis the splitting is accounted for using experimental energies. For comparison, CCSD(T) single-point energy jobs were run on halogen-formaldehyde structures that were only optimised to the MP2 level of theory, although this introduced a greater degree of error. The underlying assumption was that the MP2 structures should be quite close to that which would be converged at CCSD(T). Lastly, relaxed potential energy scans of variable Cl cluster geometries were performed at lower levels of theory. This involved varying a structural parameter (such as the bond angle between C, O, and Cl), optimising all other parameters, and determining the associated energies of these new structures. The result was a map of the PES that details information about the nature of the potential well. In an experimental context, such scans allow vibrational states to be mapped out along the PES, provided the spectral resolution is high enough.

2.4.1 Computational Data Analysis

Once the geometries of the clusters were optimised, frequency analyses performed, and energies calculated, the theoretical data could be analysed. A CBS extrapolation was used to determine highly accurate convergent energies for all halide-formaldehyde anion and halogen-formaldehyde neutral complexes. These complexes were optimised to the CCSD(T) level, with several geometries using CCSD(T) energies with MP2 geometries. A two-point extrapolation was used[54,55] between calculated energies at the CCSD(T)/aug-cc-pVQZ and CCSD(T)/aug-cc-pV5Z levels, with the underlying extrapolation theory being that the energies will converge at a complete basis set limit. In other words, as the cardinal number of the basis set increases (i.e. T=3, Q=4) to infinity the calculated energy will become more and more accurate.

To perform a CBS extrapolation, the Hartree-Fock energies (E_{HF}) and correlation energies (E_{corr}) of each basis set are treated separately (to $E_{HF}^{(\infty)}$ and $E_{corr}^{(\infty)}$ respectively) before being summed to give the CBS energy $E_{total}^{(\infty)}$ as in Equation 2.7.

$$E_{total}^{(\infty)} = E_{HF}^{(\infty)} + E_{corr}^{(\infty)} \tag{2.7}$$

$E_{HF}^{(\infty)}$ is extrapolated as follows. $E_{HF}(L)$ and $E_{HF}(L+1)$ correspond to the calculated HF energies at each basis set of cardinal number L.

$$E_{HF}^{(\infty)} = E_{HF}(L+1) + \frac{E_{HF}(L+1) - E_{HF}(L)}{c-1} \tag{2.8}$$

$$c = \frac{(L+1)^{\alpha}}{L} \tag{2.9}$$

The parameter α is generally determined through a fitting procedure, however depending on the basis sets used this value can be approximated. $E_{corr}^{(\infty)}$ can be extrapolated through an almost identical formula, although now the constant α is replaced by β.

$$E_{corr}^{(\infty)} = E_{corr}(L+1) + \frac{E_{corr}(L+1) - E_{corr}(L)}{d-1} \tag{2.10}$$

$$d = \frac{(L+1)^{\beta}}{L} \tag{2.11}$$

Both α and β, as mentioned, are determined using extrapolation plots, but for this work they can be approximated. Previous work in the Wild Group[20] used values of $\alpha = 5$ and $\beta = 3.05$. In this work these values have simplified to 5 and 3 respectively for the aug-cc-pVQZ/aug-cc-pV5Z extrapolations.

MP2 extrapolations were undertaken for all formaldehyde (QZ/5Z extrapolations) and acetone complexes (TZ/QZ extrapolations). The MP2 method was identical for that of CCSD(T) however the correlation energy was only due to the MP2 pertubation. For the CCSD(T) extrapolations the correlation energy was calculated using CCSD and CCSD(T) correlations. The MP2 CBS extrapolation applied to energies of the aug-cc-pVTZ/aug-cc-pVQZ levels for the acetone complexes was conducted with an alteration to the cardinal numbers L used as well as α and β set to 5.79 and 3.05 respectively.[56]

Upon completing the CBS at varying levels of theory for the computed clusters, the following quantities could be calculated:

1. The dissociation energy D_0: the difference in energy between the anion cluster and its individual components (e.g. $\text{Cl}^- \cdots \text{CH}_2\text{O}$ compared to Cl^- and CH_2O).
2. The adiabatic energy EA: being the difference in between the anion cluster and neutral cluster at their respective minimum energy geometries.
3. The vertical detachment energy VDE: being the difference in energies of the anion cluster and a neutral cluster at the same geometry. This is essentially simulating the photodetachment of an electron according to the Franck-Condon principle.
4. The stabilisation energy E_{stab}: being the difference in D_0 energies of the anion cluster and neutral cluster.

3 Results and Discussion

This section comprises all results from the experimental and theoretical studies. Firstly, mass spectra recorded of the various halide-containing gas mixtures will be discussed. Following on, the photoelectron spectra of $Cl^-\cdots$acetone, $Br^-\cdots$acetone, and $I^-\cdots$acetone will be presented accompanied by experimental binding and E_{stab} energies. Finally, the geometries and energies calculated computationally for each complex will be compared to the experimental data and explained.

3.1 Experimental Results

3.1.1 Mass Spectra

The mass spectrum of a gas mixture made up of CCl_4, acetone, and argon is presented in Figure 3.1. This spectrum was produced on the same day that the subsequent $Cl^-\cdots$acetone photoelectron spectrum was recorded. The unique 3:1 splitting pattern of chloride allowed the assignment of important peaks to be made, with the Cl^- peaks occurring at m/z ratios of 34.97 and 36.99. These values were used to plot an initial calibration curve. Applying the calibration to the rest of the spectrum led to the determination of $Cl^-\cdots$acetone peaks at m/z values of 93.01 and 95.03. Interestingly, as seen in the inset of Figure 3.1, the $Cl^-\cdots$acetone peaks were approximately half as intense as $Cl^-\cdots$argon (m/z of 74.97 and 76.98). Although these peaks are to be expected, the greater abundance of the argon cluster may be due to the excess of argon in the mixture. However, the large presence of bare Cl^- suggests that the formation of large amounts of clusters was unfavourable in the conditions.

Figure 3.2, a mass spectrum of a CH_2Br_2, acetone and argon mixture, displays this trend even more so. The bare bromide peaks calibrated at m/z values of 78.93 and 80.91 are significantly larger than any peak in the spectrum. Again, this may be due to unfavourable conditions for cluster formation, or that the operational parameters were set to result in an optimised Br^- signal in preference to any cluster.

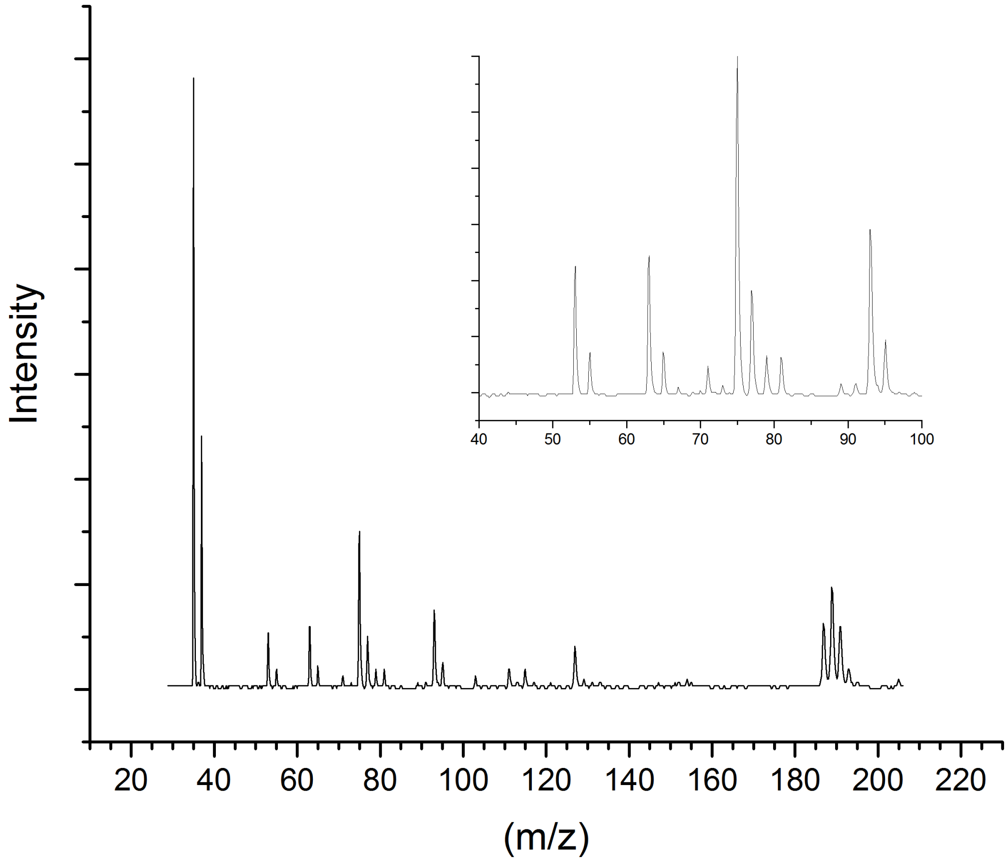

Figure 3.1: Mass spectrum of a CCl_4, acetone, and argon gas mixture.

The $Br^- \cdots$acetone peaks at m/z ratios of 136.97 and 138.99 were found to be the most intense out of any cluster species in the spectrum. The mass spectra, and subsequent photoelectron spectra were taken after a period of trialling different cooling methods for acetone, and Figure 3.2 displays the results of cooling with a dry ice-acetone bath. Although this has appeared to reduce the overall intensity of clusters, the signal itself was much more stable. This meant that a full dataset of $Br^- \cdots$acetone photoelectron spectra could be taken for the first time. Residual iodide is present at a 126.9 m/z ratio and although the intensity of the signal was weak, it could still be used to aid in calibration.

The third of the mass spectra is shown in Figure 3.3. The gas mixture was this time

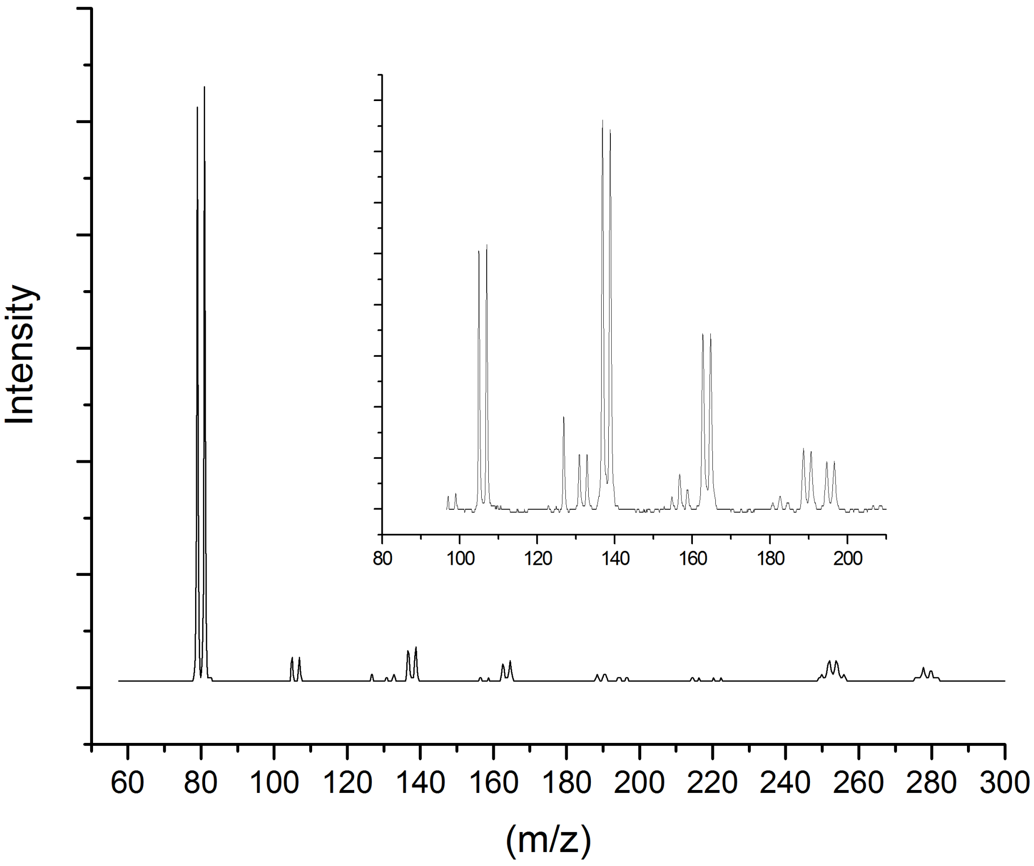

Figure 3.2: Mass spectrum of a CH_2Br_2, acetone, and argon gas mixture.

composed of CH_3I, acetone, and argon. With only the single iodide peak at a m/z ratio of 126.91, this spectrum was difficult to initally calibrate. However, some residual bromide species including the bare Br^- peaks were found in the spectrum. Although the bare peaks are not included in the spectrum, a clear splitting pattern at m/z values of 118.9 and 121.0 is observable, indicating a bromide cluster (most likely bromide-argon). These bromide peaks were used to calibrate the spectrum. The $I^- \cdots$acetone cluster is observable at a 184.95 m/z ratio, with iodide clusters with water (144.9 m/z), argon (166.9 m/z) and CH_3I (268.8 m/z) being more intense. This did not affect the photoelectron experiments, however, as the relatively isolated peak could be honed in on with ease.

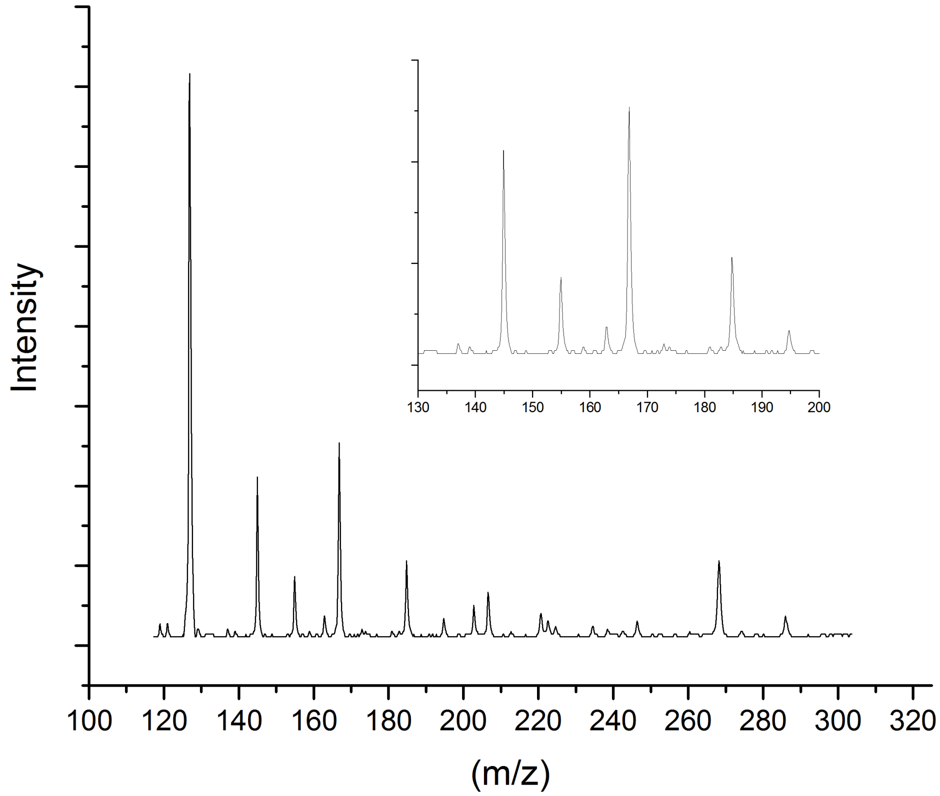

Figure 3.3: Mass spectrum of a CH_3I, acetone, and argon gas mixture.

3.1.2 Photoelectron Spectra

Photoelectron spectra were recorded of the Cl$^{-}\cdots$acetone, Br$^{-}\cdots$acetone, and I$^{-}\cdots$acetone clusters for the first time and are presented here. The contents of Table 3.1, a summary of the experimental binding energies of each cluster, bare halide, and resulting E_{stab} values, will be discussed in conjunction with each spectrum.

Table 3.1: Experimentally determined binding energies for halide-acetone complexes (eV)

	Cl$^-$	Br$^-$		I$^-$	
	$^2P_{3/2}$	$^2P_{3/2}$	$^2P_{1/2}$	$^2P_{3/2}$	$^2P_{1/2}$
Bare	3.694	3.364	3.821	3.059	4.002
Complex	4.377	3.933	4.394	3.511	4.466
E_{stab}	0.683	0.569	0.573	0.452	0.464

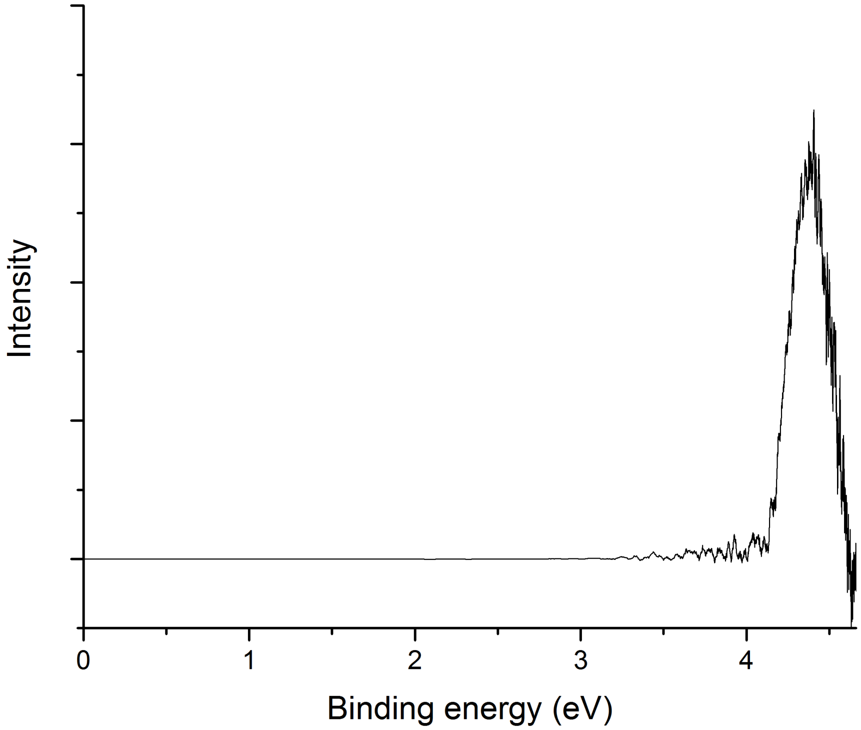

Figure 3.4: Photoelectron spectrum of the $\text{Cl}^- \cdots$acetone complex.

The E_{stab} values are experimentally determined as the difference in binding energies between the bare halide and the complex. Computationally, E_{stab} corresponds to the difference in D_0 energies between the anion and neutral complex. A comparison between the experimental and computational values will be undertaken in the computational results section. What is apparent immediately from Table 3.1 is that E_{stab} decreases as halide size increases. This means that the forces of attraction in the van der Waals clusters are greater the smaller the halide is. Additionally, the experimental E_{stab} values are relatively large. For comparison, previous research in the Wild group found an E_{stab} of 0.16 eV for the $\text{Cl}^- \cdots \text{CO}$ complex.[33] The large stability of the halide-acetone clusters may have repercussions in an atmospheric environment, with the formation of such clusters seeming favourable and likely leading to greater atmospheric lifetimes and reactivity.

Figure 3.4 shows a recorded photoelectron spectrum of the $Cl^{-}\cdots$acetone complex. This complex has a binding energy of approximately 4.377 eV and the largest experimental E_{stab} value of any studied cluster in this work at 0.683 eV. The splitting of the Cl^{-} $^2P_{3/2}$ and $^2P_{1/2}$ states is not apparent in this spectrum, due to the low resolution of the apparatus.

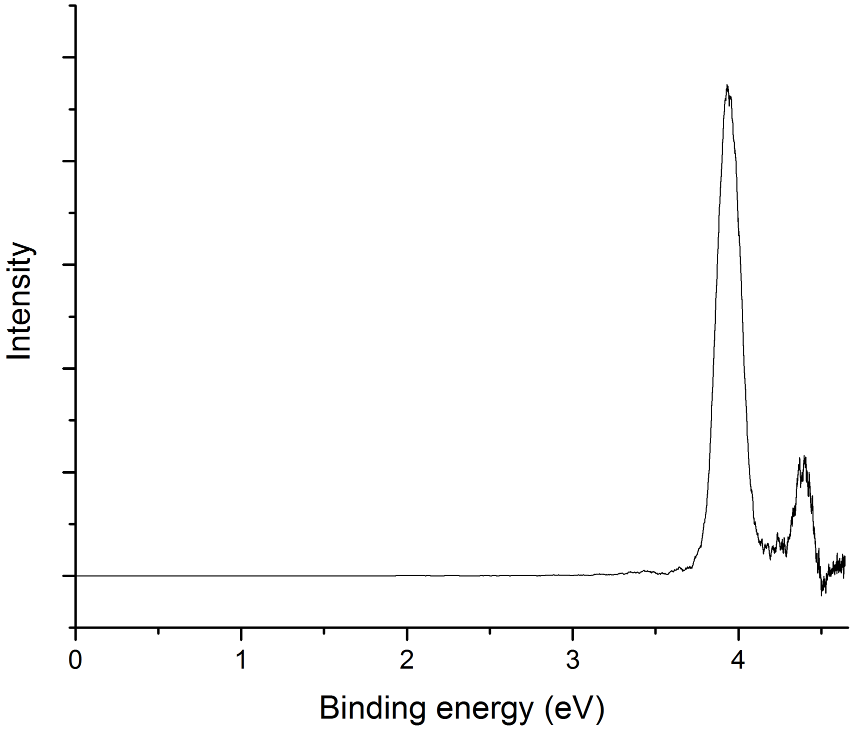

Figure 3.5: Photoelectron spectrum of the $Br^{-}\cdots$acetone complex.

The Br^{-} $^2P_{3/2}$ and $^2P_{1/2}$ splitting is apparent, however, in the photoelectron spectrum of $Br^{-}\cdots$acetone shown in Figure 3.5. This complex was found to have binding energies of 3.933 eV ($^2P_{3/2}$) and 4.393 eV ($^2P_{1/2}$) with respective stabilisation energies of 0.569 eV and 0.573 eV.

Lastly, the photoelectron spectrum of $I^{-}\cdots$acetone is displayed in Figure 3.6. This complex has the lowest experimentally determined E_{stab} values of this work (0.452 eV and 0.464 eV for the $^2P_{3/2}$ and $^2P_{1/2}$ states respectively). As to be expected based on

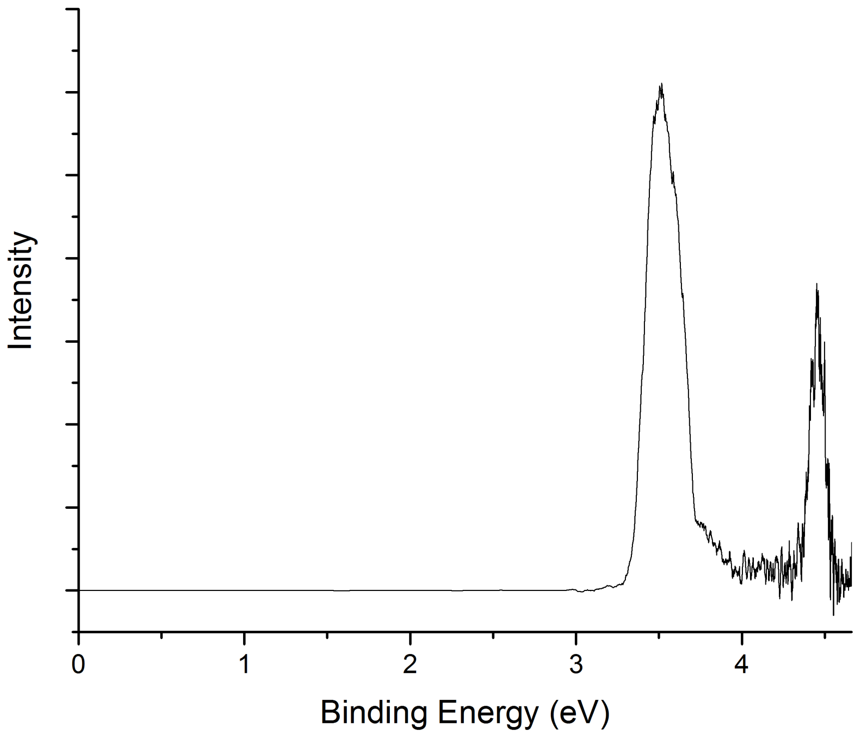

Figure 3.6: Photoelectron spectrum of the $I^{-}\cdots$acetone complex.

spectra of the bare halides, the $I^{-}\cdots$acetone complex also has the greatest degree of spin-orbit coupling, corresponding to binding energies of 3.511 eV and 4.466 eV. There is also a notable amount of noise in between each peak, most likely due to the high power of the laser used. However, this shoulder on the right hand side of the main peak could be a result of vibrational structure. Recording higher resolution spectra through the SEVI apparatus in the future will allow this feature to be investigated.

The experimental results will be rationalised next through a discussion of calculated geometries and energies of the investigated complexes, as well as for fluoride-acetone complexes. Although no halide-formaldehyde photoelectron spectra were taken during this work, it remains a top priority as future work and as such the computational data relating to these complexes will also be presented.

3.2 Computational Results

As a foreword, all halide-acetone and halogen-acetone complexes were optimised to the MP2/aug-cc-pVTZ (aug-cc-pV(T+d)Z for Cl and aug-cc-pVTZ PP for Br and I) level with energy extrapolations conducted between the aug-cc-pVTZ and aug-cc-PVQZ basis sets at the same level of theory. With the exception of the C-appended neutral structures, all halide-formaldehyde and halogen-formaldehyde geometries were optimised at the CCSD(T)/aug-cc-pVTZ (and related custom basis sets) level with the basis set extrapolation involving aug-cc-pVQZ and aug-cc-pV5Z energies.

3.2.1 Fluoride-Acetone Complexes

The geometries of all halide-acetone anion complexes are very similar. Figure 3.7 shows the only anion structure computed for $F^{-}\cdots C_3H_6O$. The geometry is of C_s symmetry with the fluoride sitting out of plane relative to the acetone molecule (making an angle of 143.4° with the carbonyl bond). The neutral structure (Figure 3.8) has the fluorine seemingly appended to the O atom of the carbonyl bond at a distance of 2.367 Å at an angle of 120.1° with the carbonyl bond. This structure also has C_s symmetry with the halogen lying in plane with the acetone molecule.

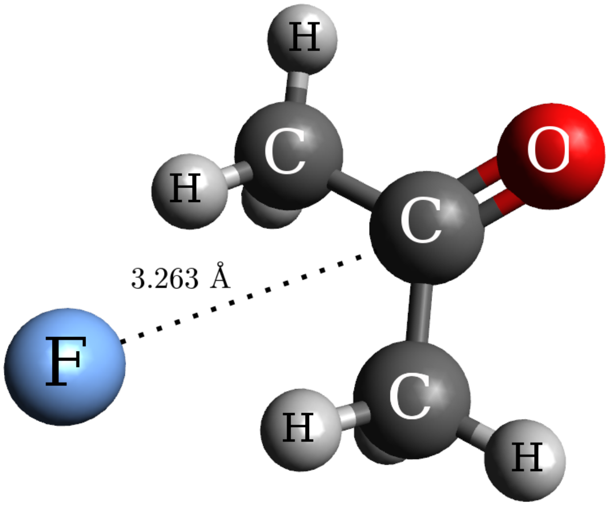

Figure 3.7: C_s structure of $F^{-}\cdots C_3H_6O$ computed to MP2/aug-cc-pVTZ.

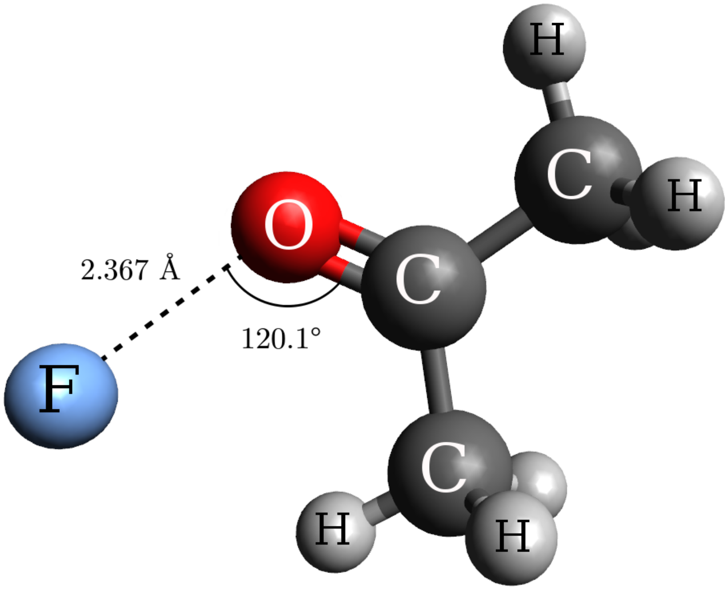

Figure 3.8: C_s structure of F$\cdots$C$_3$H$_6$O computed to MP2/aug-cc-pVTZ.

Although no experiments were conducted on fluoride complexes, the computational energies obtained can be of use in predicting experimental parameters, should photoelectron spectra of $F^{-}\cdots C_3H_6O$ complexes be taken in the future. The energies derived from the MP2 basis set extrapolation are shown in Table 3.2. For the computational results, the VDE is listed alongside the anion energies while the EA is listed alongside the neutral geometry energies. This convention will be used throughout the presentation of computational data. As will be seen with the $F^{-}\cdots CH_2O$ complex, the MP2 calculations appear to overestimate the VDE values for the fluoride complexes. However, of note are the EA values as well as the calculated E_{stab}, which should provide reasonable experimental agreement despite the error introduced using MP2 calculations. The MP2 predictions appear to fit the experimental observation that E_{stab} increases with decreasing halide size.

Table 3.2: Computational energies determined for fluoride-acetone complexes.

	D_0	VDE (eV)		EA (eV)		E_{stab}
	(kJ mol^{-1})	$^2P_{3/2}$	$^2P_{1/2}$	$^2P_{3/2}$	$^2P_{1/2}$	(eV)
$F^{-}\cdots C_3H_6O$	90.7	5.609	5.660	-	-	-
$F\cdots C_3H_6O$	8.0	-	-	4.242	4.292	0.857

3.2.2 Chloride-Acetone Complexes

The results of calculations conducted on chloride-acetone complexes will provide the first comparison between the experimental and theoretical results of this work. Firstly, the anion complex was converged to a similar geometry to that of $F^{-}\cdots C_3H_6O$, as shown in Figure 3.9. The anion geometry has C_s symmetry with a mirror plane intersecting the Cl, central C, and O atoms. The $Cl^{-}\cdots C$ distance has extended to 3.914 Å while the angle made with the carbonyl bond has slightly increased to 144.1° from that of the $F^{-}\cdots C_3H_6O$ complex.

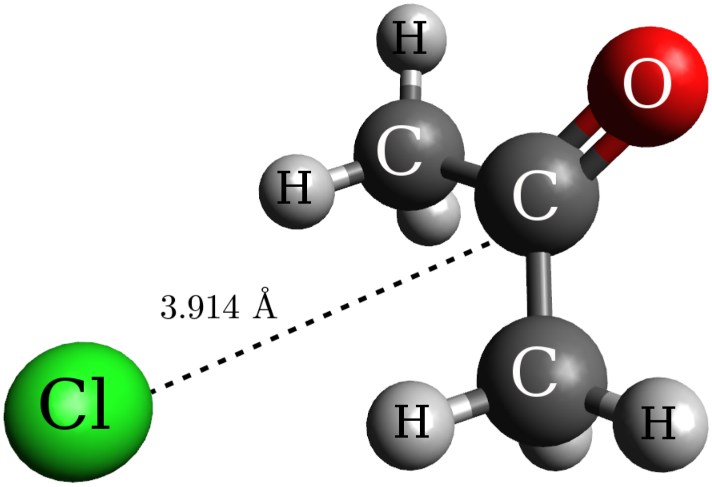

Figure 3.9: C_s structure of $Cl^{-}\cdots C_3H_6O$ computed to MP2/aug-cc-pV(T+d)Z.

Again, only one neutral geometry was found for the $Cl\cdots C_3H_6O$ complex, with all other stationary points proving to be transition states. Figure 3.10 details this C_s geometry, with interesting features being a $Cl\cdots O$ distance of 2.510 Å as well as the halogen angle with the carbonyl bond extending to 121.6°. Both of these structural parameters show an increase to those of the neutral $F\cdots C_3H_6O$ complex.

Computational energies determined using the MP2 basis set extrapolation are detailed in Table 3.3, as well as a comparison to the experimentally determined energies. The binding energy from experiment is listed under the VDE column. One example of the additional error brought in by MP2 calculations is demonstrated in the table. The computational values for the EA are slightly higher than that of the VDE, which fundamentally should not happen, as the EA is the transition involving the smallest binding energy of the system. Considering this occurred after zero-point energies were corrected for, the error is likely due to an overestimation of these energies by the MP2 formulae.

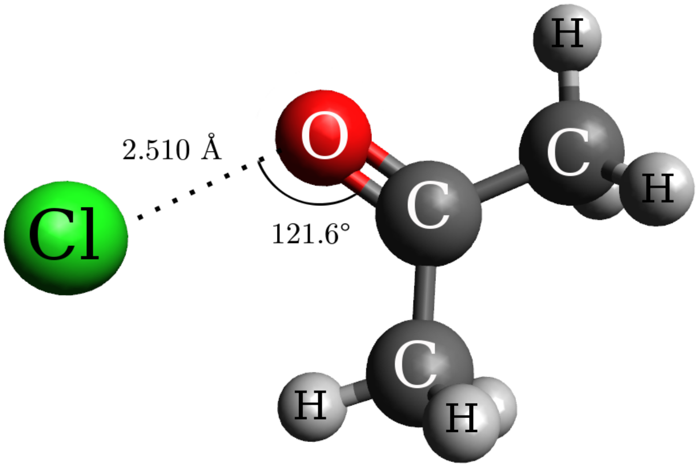

Figure 3.10: C_s structure of $Cl \cdots C_3H_6O$ computed to MP2/aug-cc-pV(T+d)Z.

However, the calculated VDE and EA provide a reasonable estimate of the experimental binding energy, and the E_{stab} value is also close. Further calculations at the CCSD(T) level of theory would provide interesting comparisons to both the existing MP2 energies as well as the experimental data.

Table 3.3: Relevant energies determined for the chloride-acetone complexes.

	D_0	VDE (eV)		EA (eV)		E_{stab}
	(kJ mol^{-1})	$^2P_{3/2}$	$^2P_{1/2}$	$^2P_{3/2}$	$^2P_{1/2}$	(eV)
$Cl^- \cdots C_3H_6O$	59.2	4.020	4.130	-	-	-
$Cl \cdots C_3H_6O$	20.4	-	-	4.026	4.136	0.402
Experimental	-	4.337	-	-	-	0.683

3.2.3 Bromide-Acetone Complexes

The bromide-acetone anion complex optimised to the MP2/aug-cc-pVTZ PP level of theory features an increased distance between the halide and the central C atom of acetone, although maintains a similar geometry to those previously seen. The neutral complex optimised to the same level again shows an increase in the Br $\cdots$ O distance as well as a slight increase in the angle made with the carbonyl bond to 122.1°. Figures 3.11 and 3.12 display these structures.

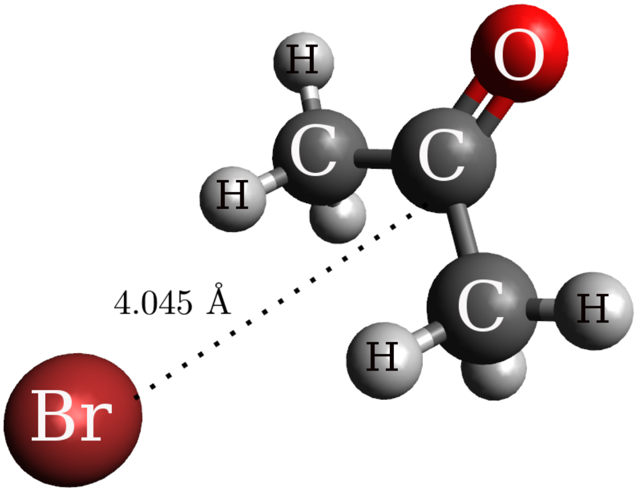

Figure 3.11: C_s structure of $Br^- \cdots C_3H_6O$ computed to MP2/aug-cc-pVTZ PP.

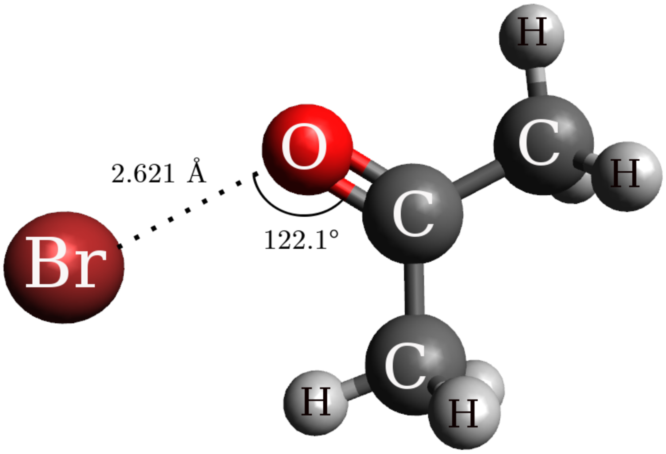

Figure 3.12: C_s structure of $Br \cdots C_3H_6O$ computed to MP2/aug-cc-pVTZ PP.

The important energies determined by both computation and experiment are listed in Table 3.4. Again, the MP2 extrapolation provides a poor estimate of the VDE. However, as with the previous calculations on the chloride-acetone complexes, there is reasonable agreement between the experimental binding energies and EA, as well as E_{stab} values from both theory and experiment. The predicted E_{stab} values tend to underestimate the experimental value by 2-300 meV, although provide a good estimate of the scale of the experimental E_{stab}.

Table 3.4: Relevant energies determined for the bromide-acetone complexes.

	D_0	VDE (eV)		EA (eV)		E_{stab}
	(kJ mol^{-1})	$^2P_{3/2}$	$^2P_{1/2}$	$^2P_{3/2}$	$^2P_{1/2}$	(eV)
$Br^{-}\cdots C_3H_6O$	58.7	6.419	6.875	-	-	-
$Br\cdots C_3H_6O$	26.1	-	-	3.693	4.150	0.337
Experimental	-	3.364	3.933	-	-	0.569 ($^2P_{3/2}$) 0.573 ($^2P_{1/2}$)

Additionally, the theoretical E_{stab} values so far display the same experimental trend of decreasing with increasing halide size. Thus the MP2 calculations can prove to show a reasonable estimate of experimental trends (with the exception of VDE). The D_0 values for the bromide-acetone complexes are similar to that of the chloride complexes with slight variations. The dissociation energies are relatively high compared to values previously obtained for complexes in the Wild group (to be discussed in more depth later) and the stability of these complexes could be a contributing factor in atmospheric reactions. This is especially true for the neutral complexes, with the neutral O-appended structures thought to be a pre-reaction adduct in the hydrogen abstraction of formaldehyde (and acetone by extension) by halogen atoms.[13]

3.2.4 Iodide-Acetone Complexes

The $I^{-}\cdots C_3H_6O$ anion complex completes the trend of C_s halide-acetone anion structures. The iodide sits out of plane at an angle of 145.3° relative to the carbonyl bond, and this angle has only varied slightly between each halide geometry. The $I^{-}\cdots C$ distance again increased to 4.313 Å, showing that as halide size increases, so too does this parameter for halide-acetone complexes. The neutral O-appended structure increases the halogen $\cdots$ O distance to 2.833 Å, with the angle made with the carbonyl bond slightly widening to 124.3°.

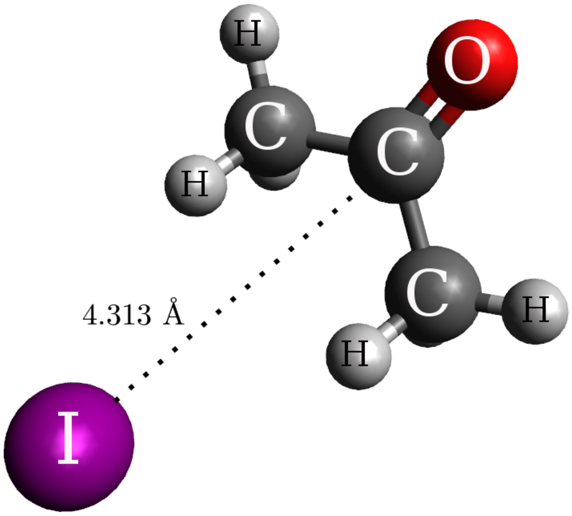

Figure 3.13: C_s structure of $I^{-}\cdots C_3H_6O$ computed to MP2/aug-cc-pVTZ PP.

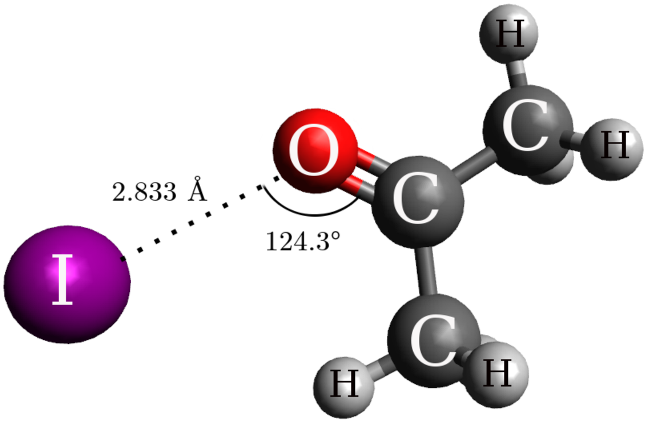

Figure 3.14: C_s structure of $I\cdots C_3H_6O$ computed to MP2/aug-cc-pVTZ PP.

The computational energies extracted using the MP2 basis set extrapolation show by far the best experimental agreement with the iodide-acetone complexes. The calculated E_{stab} value decreases from those presented for the other halide complexes, displaying the trend that E_{stab} decreases with increasing halide size. Computational values of EA and E_{stab} continue to underestimate the respective experimental energies by 2-300 meV, with this trend being consistent for all acetone complexes. With this in mind however, the MP2 results provide good experimental estimates.

Table 3.5: Relevant energies determined for the iodide-acetone complexes.

	D_0	VDE (eV)		EA (eV)		E_{stab}
	(kJ mol^{-1})	$^2P_{3/2}$	$^2P_{1/2}$	$^2P_{3/2}$	$^2P_{1/2}$	(eV)
$I^{-}\cdots C_3H_6O$	54.3	3.548	4.491	-	-	-
$I\cdots C_3H_6O$	29.4	-	-	3.309	4.252	0.258
Experimental	-	3.511	4.466	-	-	0.452 ($^2P_{3/2}$) 0.464 ($^2P_{1/2}$)

The VDE calculated shows excellent experimental agreement, although the inconsistent results from the previous complexes reduces this reliability somewhat. Analysis of the computational data allows the experimental observations to be rationalised. For example, E_{stab} was shown to decrease both experimentally and computationally as the size of the halide increases. In terms of the computational results, this can be rationalised as the anion complex D_0 growing smaller (becoming less stable) with increasing halide size while the neutral complex D_0 grows larger with halogen size. The result is a decrease in the difference between the anion and neutral D_0 values, leading to decreased E_{stab} values determined.

3.2.5 Fluoride-Formaldehyde Complexes

The geometry of the $F^- \cdots CH_2O$ anion complex was optimised to the CCSD(T)/aug-cc-pVTZ level of theory. The single anion structure takes shape with the F^- anion appended to a H on CH_2O, as shown in Figure 3.15. This geometry is unique among all complexes studied in this work, as no other anion was found to append to a single hydrogen (with the latter halide-formaldehyde anion clusters the appendage is to both hydrogens). The distance between F^- and the closest H is 1.659 Å, and although this distance is closer than expected it is much greater than the largest H−F covalent bonds of approximately 1.15 Å.[57] Therefore it can be said that this anion structure is a van der Waals cluster, with the bonding motif best described as hydrogen bonding. Additionally, the distance of the C−H bond closest to the fluoride increased to 1.127 Å from a value of 1.103 Å of the bare formaldehyde.

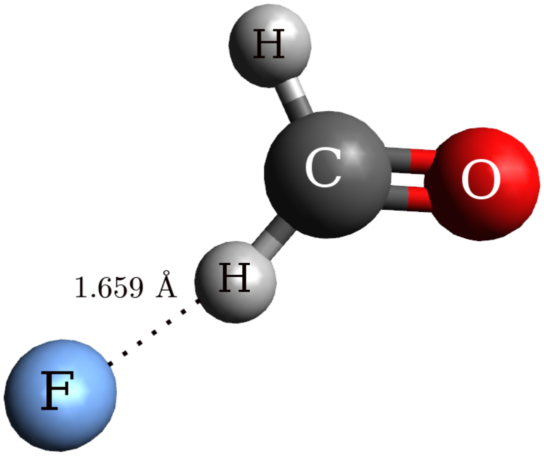

Figure 3.15: C_s structure of $F^- \cdots CH_2O$ computed to the CCSD(T)/aug-cc-pVTZ level.

Only one neutral structure was found for the $F \cdots CH_2O$ complex, similar in shape to that described by Beukes et al.[13] The other halogen-formaldehyde complexes were found to have another neutral geometry shape, although for the fluorine complex this type of structure was revealed to be a transition state during frequency analysis. As seen in Figure 3.16, the $F \cdots CH_2O$ neutral complex is appended to the O atom with a distance of 2.040 Å and makes an angle of 100.3^o with the C=O bond. Interestingly, this structure deviated highly upon CCSD(T)/aug-cc-pVTZ convergence, with the MP2/aug-cc-pVTZ geometry having a F$\cdots$O distance of 2.443 Å and an angle with the C=O bond of 102.4^o. This was believed to be a result of the CCSD(T) algorithm, with both Gaussian 09 and CFOUR converging towards the same CCSD(T) geometry. Additionally, the CCSD(T) geometry could not be converged at MP2/aug-cc-pVTZ to determine if the structures were indeed different minima. For comparison, Beukes et al.[13] described an MP2 shape with a F $\cdots$ O distance of 2.519 Å and an angle with C=O of 99.7^o. The slight differences are likely due to the tighter convergence criteria used in this work, and the larger basis sets leading to a contraction in bond lengths.

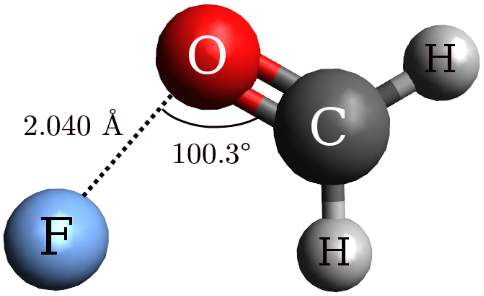

Figure 3.16: C_s structure of F$\cdots$CH$_2$O computed to the CCSD(T)/aug-cc-pVTZ level.

Important energies determined from the CCSD(T) and MP2 CBS extrapolations are presented in Table 3.6. The CCSD(T) energies in particular will provide predictions of photoelectron spectral data for the $F^- \cdots CH_2O$ complex, should this complex be studied in the future. This work presents the first computations conducted on the $F^- \cdots CH_2O$ anion complex as well as providing the first calculations of the $F \cdots CH_2O$ neutral complex at the CCSD(T)/aug-cc-pVTZ level of theory.

Table 3.6: Important energies of the fluoride-formaldehyde complexes.

		D_o	VDE (eV)		EA (eV)		E_{stab}
	Level of theory	(kJ mol^{-1})	$^2P_{3/2}$	$^2P_{1/2}$	$^2P_{3/2}$	$^2P_{1/2}$	(eV)
$F^- \cdots CH_2O$	MP2	74.6	4.859	4.909	-	-	-
	CCSD(T)	77.2	4.118	4.168	-	-	-
$F \cdots CH_2O$	MP2	23.8	-	-	3.878	3.928	0.527
	CCSD(T)	15.9	-	-	4.003	4.053	0.635

3.2.6 Chloride-Formaldehyde Complexes

Shown in Figures 3.17-3.19 are the computed structures for the $Cl^{-}\cdots CH_2O$ anion and $Cl\cdots CH_2O$ neutral complexes. The anion and O-appended (Figure 3.18) geometries have been optimised to CCSD(T)/aug-cc-pV(T+d)Z while the C-appended structure (Figure 3.19) has been optimised to MP2/aug-cc-pV(T+d)Z.

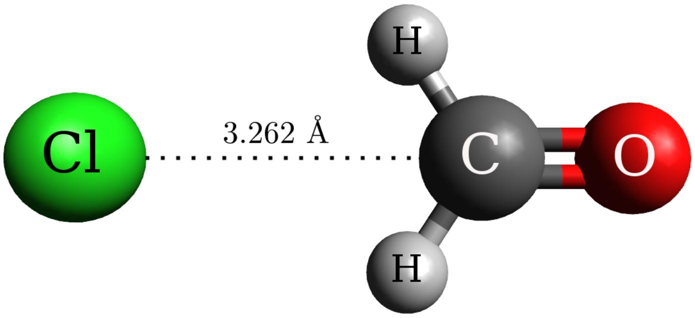

Figure 3.17: C_{2v} structure of $Cl^{-}\cdots CH_2O$ computed to the CCSD(T)/aug-cc-pV(T+d)Z level.

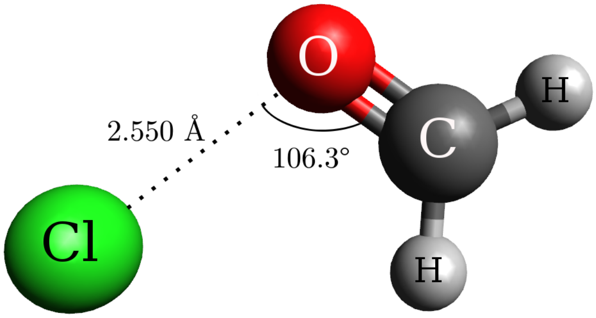

Figure 3.18: C_s structure of neutral $Cl\cdots CH_2O$ computed to CCSD(T)/aug-cc-pV(T+d)Z.

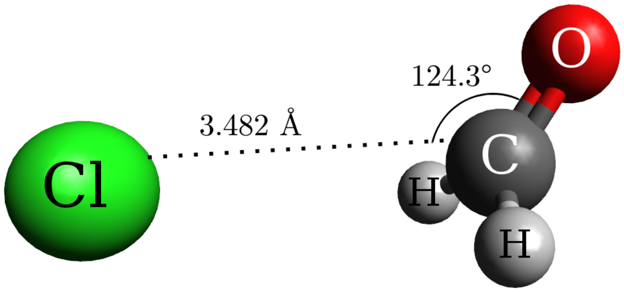

Figure 3.19: Second C_s structure of $Cl\cdots CH_2O$ computed to MP2/aug-cc-pV(T+d)Z.

The anion structure begins the trend for the remainder of the halide-formaldehyde complexes of featuring the halide positioned an equal distance from each H atom in a C_{2v} geometry. The O-appended C_s geometry of the neutral complex is characteristic of other halogen-formaldehyde neutral complexes with a similar geometry to that calculated for $\mathrm{F} \cdots \mathrm{CH_2O}$ but with a greater halogen$\cdots$O distance (to 2.550 Å) and increased angle made with the C=O bond (100.3° to 106.3°). Beukes et al.[13] described a distance of 2.716 Å and a respective angle of 108.5° with the C=O bond. The tighter convergence criteria used in this work and the greater level of theory should make the structure reported here more reliable.

A second neutral structure was also computed, forming a C_s symmetry geometry with a mirror plane through Cl, C, and O. The D_0 energies listed in Table 3.7 suggest that the O-appended structure is more stable relative to the C-appended neutral species. Additionally, there is a marked decrease in D_0 energies from that of the fluoride-formaldehyde complexes. The CCSD(T) energies of the C-appended structure were calculated using the MP2/aug-cc-pV(T+d)Z geometry.

Table 3.7: Important energies of the chloride-formaldehyde complexes.

		D_0	VDE (eV)		EA (eV)		E_{stab}
	Level of theory	(kJ mol^{-1})	$^2P_{3/2}$	$^2P_{1/2}$	$^2P_{3/2}$	$^2P_{1/2}$	(eV)
$\mathrm{Cl^-}\cdots\mathrm{CH_2O}$	MP2	49.4	4.072	4.181	-	-	-
	CCSD(T)	49.6	4.072	4.181	-	-	-
$\mathrm{Cl}\cdots\mathrm{CH_2O}$	MP2	9.9	-	-	3.990	4.100	0.410
(O-appended)	CCSD(T)	15.0	-	-	3.967	4.076	0.358
$\mathrm{Cl}\cdots\mathrm{CH_2O}$	MP2	2.0	-	-	4.107	4.217	0.492
(C-appended)	CCSD(T)	1.1	-	-	4.111	4.220	0.502

A point of interest in discussing these geometries arose with Gruber-Stadler et al.[14] confirming the existence of the structure in Figure 3.18, but stating it does not lie on the minimum energy path of the hydrogen abstraction of formaldehyde by the Cl atom. Instead, the pre-reaction adduct structure is said to resemble the anion complex geometry, albeit with the Cl atom slightly further away. Computing this structure at the MP2/aug-cc-pVTZ level and conducting a frequency analysis revealed it to instead be a transition state. Therefore, the pre-reaction adduct structure proposed by Gruber-Stadler et al.[14] may very well lie on the minimum energy path of the reaction, but certainly not as a pre-reaction adduct.

The relevant energies of the chloride-formaldehyde complexes are displayed in Table 3.7. It is hoped that the CCSD(T) calculations (in particular for the anion and O-appended neutral complexes) will provide accurate estimates of the experimental photoelectron spectrum of $Cl^{-}\cdots CH_2O$ when it is taken. The D_0 values have markedly decreased in comparison to the fluoride-formaldehyde complexes, although this is to be expected. Firstly, the anion complex geometries are different, and secondly, the halide size has increased. As observed with the acetone complexes, the D_0 values for the anion clusters decrease with increasing halide size, while increase slightly for the neutral clusters with halogen size. This seems to suggest that the forces of attraction are greater for the smaller halides in the anion complexes, while weaker for these smaller halides in the neutral complexes, potentially due to the larger halogen size increasing the dispersion interaction.

The C_{2v} anion structure of Figure 3.17 was optimised similarly for both bromide and iodide complexes, yet could not be converged for the fluoride anion complex. Conversely, the anion structure of $F^{-}\cdots CH_2O$ could not be converged for the other halides. In an attempt to rationalise the difference and map out what was occurring in terms of potential energy surfaces, a scan of the $Cl^{-}\cdots CH_2O$ anion complex was performed. The scan, shown in Figure 3.20, effectively revolved the chloride ion around the formaldehyde molecule (while remaining in plane), optimising all other parameters as the calculation went on.

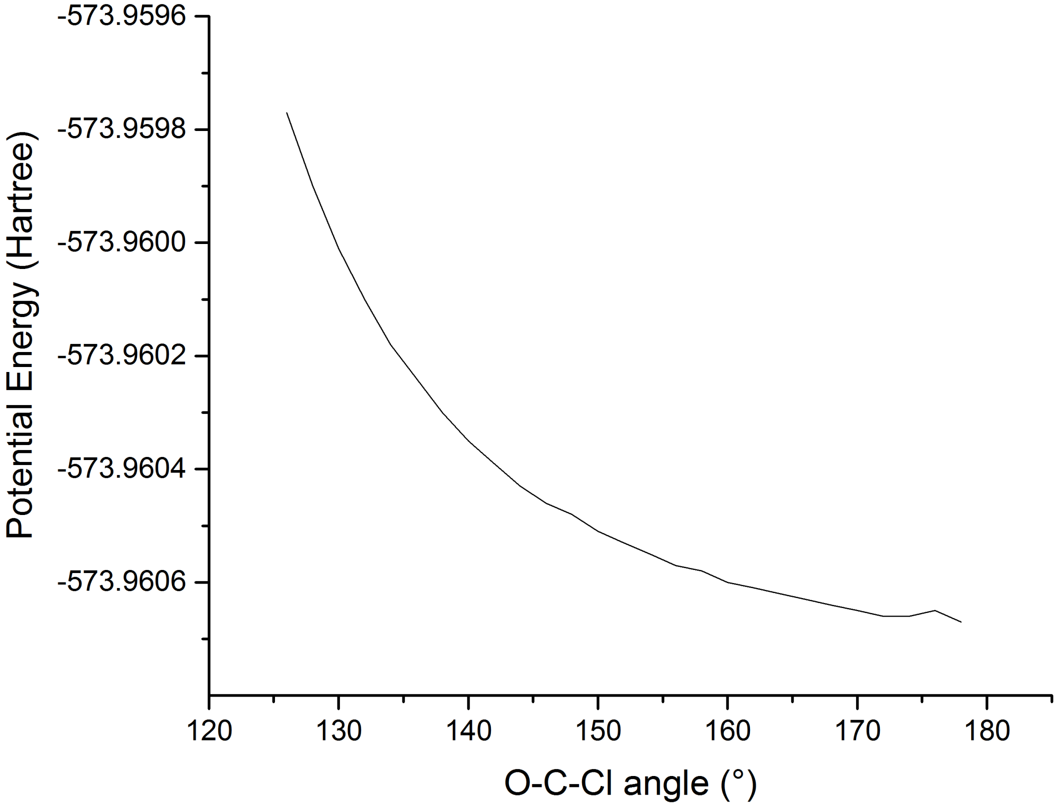

Figure 3.20: Scan of the O=C$\cdots$Cl$^-$ angle of the Cl$^-\cdots$CH$_2$O complex at MP2/aug-cc-pVDZ.

As can be seen, as the chloride ion approached each H atom to a position similar to the F$^-\cdots$CH$_2$O geometry (away from the 180° minimum point), the potential energy of the system increased, indicating that appending to a single hydrogen is unfavourable for the heavier halides. Instead, positioning itself in between each H atom in a C_{2v} structure seems to provide an equilibrium point.

3.2.7 Bromide-Formaldehyde Complexes

The optimised structures for the bromide-formaldehyde anion and bromine-formaldehyde neutral structures are provided in Figures 3.21-3.23. As for the previous chloride complexes, only a single anion structure was converged, being a similar C_{2v} shape. The neutral complexes also include an O-appended and C-appended geometries.

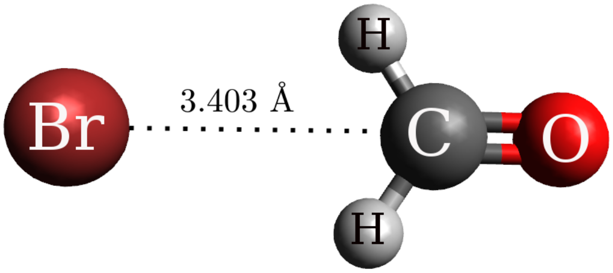

Figure 3.21: C_{2v} structure of $Br^{-}\cdots CH_2O$ computed to the CCSD(T)/aug-cc-pVTZ PP level.

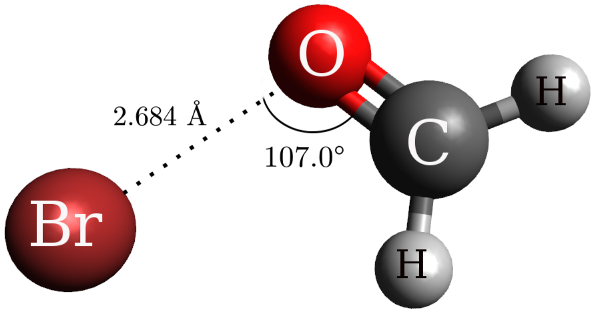

Figure 3.22: C_s structure of $Br\cdots CH_2O$ computed to the CCSD(T)/aug-cc-pVTZ PP level.

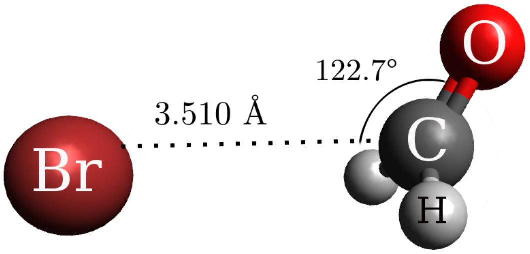

Figure 3.23: Second C_s structure of $Br\cdots CH_2O$ computed to the MP2/aug-cc-pVTZ PP level.

In relation to the previous halide-formaldehyde complexes, the anion structure features a larger distance between the C atom and the halide. The neutral O-appended structure also includes slight increases of the halogen distances well as the angle made with the carbonyl bond. This is also observed for the C-appended $Br \cdots CH_2O$ geometry, although the angle made with the carbonyl bond has actually decreased. The geometry described by Beukes et al.[13] has the Br atom positioned slightly further away than reported in Figure 3.22 with an angle with the carbonyl of 109.6°. These differences are believed to be a result of the tighter optimisation conditions used here. This work presents the first calculations on this cluster at the CCSD(T)/aug-cc-pVTZ PP level.

Table 3.8: Important energies of the bromide-formaldehyde complexes.

		D_0	VDE (eV)		EA (eV)		E_{stab}
	Level of theory	(kJ mol^{-1})	$^2P_{3/2}$	$^2P_{1/2}$	$^2P_{3/2}$	$^2P_{1/2}$	(eV)
$Br^- \cdots CH_2O$	MP2	46.6	3.836	4.293	-	-	-
	CCSD(T)	46.1	3.833	4.290	-	-	-
$Br \cdots CH_2O$	MP2	12.5	-	-	3.688	4.144	0.354
(O-appended)	CCSD(T)	16.0	-	-	3.672	4.129	0.312
$Br \cdots CH_2O$	MP2	3.4	-	-	3.814	4.271	0.448
(C-appended)	CCSD(T)	2.2	-	-	3.814	4.271	0.455

The CCSD(T) values of Table 3.8 should provide accurate representations of experimental data, should the photoelectron spectrum of $Br^- \cdots CH_2O$ be taken in the future. The D_0 value of the anion complex has decreased from that of $Cl^- \cdots CH_2O$, while the neutral D_0 energies have increased. This trend was also observed as halide size increased for the acetone complexes. The end result of this is a decrease in the values of E_{stab}. The MP2 data agrees largely with the CCSD(T) calculations (the exact agreement of the C-appended EA values is pure coincidence) apart from the neutral D_0 values. Interestingly, the MP2 calculation of the VDE did not overestimate the value as per the acetone calculations.

The greater stability of the O-appended neutral structure relative to the C-appended structure suggests it is more relevant in an atmospheric context, and is very likely the shape of the pre-reaction adduct in the hydrogen abstraction of formaldehyde, as has been suggested.[13] The next step in analysing these data for the bromide-formaldehyde complexes is to converge the C-appended structure at the CCSD(T)/aug-cc-pVTZ PP level of theory, and compare the data to experimental photoelectron spectra.

3.2.8 Iodide-Formaldehyde Complexes

The iodide-formaldehyde computationally determined geometries are shown in Figures 3.24-3.26. The structures are similar to those of the chloride and bromide complexes, albeit with greater halide distances to the formaldehyde molecule.

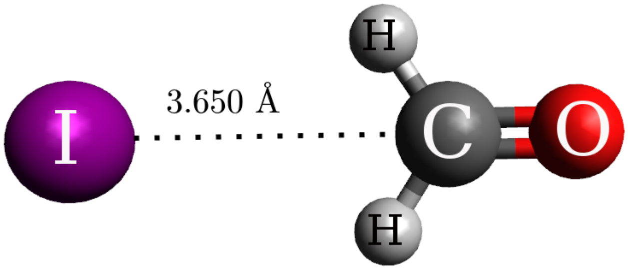

Figure 3.24: C_{2v} structure of $I^{-} \cdots CH_2O$ computed to the CCSD(T)/aug-cc-pVTZ PP level.

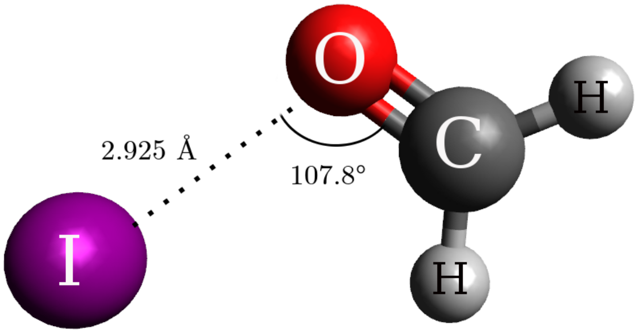

Figure 3.25: C_s structure of $I \cdots CH_2O$ computed to the CCSD(T)/aug-cc-pVTZ PP level.

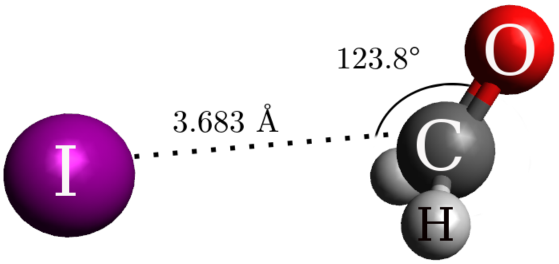

Figure 3.26: C_s structure of $I \cdots CH_2O$ computed to the MP2/aug-cc-pVTZ PP level.

These three geometries have been converged for the Cl^-, Br^- and I^- complexes with formaldehyde. The fluoride complexes were the exception to the halide trend, although did feature an O-appended neutral geometry. It can be seen that this type of neutral structure was optimised for all clusters studied in this work, displaying a universal minimum geometry among the halogen complexes with simple carbonyls. Additionally, the work on the $I \cdots CH_2O$ geometry of Figure 3.25 is novel, with Beukes et al.[13] not including iodine in their study of halogen-formaldehyde pre-reaction adducts.

Table 3.9: Important energies of the iodide-formaldehyde complexes.

	Level of theory	D_0 (kJ mol^{-1})	VDE (eV) $^2P_{3/2}$	VDE (eV) $^2P_{1/2}$	EA (eV) $^2P_{3/2}$	EA (eV) $^2P_{1/2}$	E_{stab} (eV)
$I^- \cdots CH_2O$	MP2	44.5	3.460	4.402	-	-	-
	CCSD(T)	43.3	3.457	4.399	-	-	-
$I \cdots CH_2O$	MP2	16.8	-	-	3.464	4.407	0.287
(O-appended)	CCSD(T)	17.9	-	-	3.318	4.261	0.263
$I \cdots CH_2O$	MP2	3.2	-	-	3.452	4.395	0.428
(C-appended)	CCSD(T)	3.9	-	-	3.466	4.408	0.409

The computational energies of the iodide-formaldehyde complexes show some interesting results. The energies calculated of the anion cluster as well as the neutral O-appended complex at the CCSD(T)/aug-cc-pVTZ PP level of theory are most relevant to potential experimental data due to the high accuracy to which they were computed. The C-appended $I \cdots CH_2O$ structure (like similar structures for the chloride and bromide complexes) was only optimised to the MP2/aug-cc-pVTZ PP level of theory, with the CBS extrapolation performed using CCSD(T)/aug-cc-pVTZ PP and QZ PP energies (as opposed to QZ/5Z for all other formaldehyde complexes). This is the likely reason why the CCSD(T) EA values are larger than the VDE values for the C-appended complex. In other words, a fair amount of error has been introduced for the CCSD(T) calculations for this complex due to the original MP2 geometry being used as well as only a TZ/QZ extrapolation.

For comparison however, the MP2 EA values for the C-appended geometry are still very close to the VDE numbers. This may suggest that the shape of the potential energy curves of the anion and the C-appended complexes are offset in a way to provide a VDE close to the EA. The E_{stab} values have again decreased from the smaller halides, continuing the trend seen throughout this work's theoretical and experimental studies. The VDE calculations for the formaldehyde clusters have been more well behaved than for the acetone clusters, even at the MP2 level. A revisiting of these acetone calculations using different basis sets and levels of theory may help to elucidate the problem of farfetched energies.

3.2.9 Summary of Computational Results

The halide-acetone complexes all converged to a single similar C_s geometry. As the halide size increased so too did the distance between the acetone molecule and the halide itself. The neutral complexes converged to a minimum structure that appeared to have the halogen appended to the O atom of the acetone, lying in plane with the carbonyl bond with a C_s symmetry. A similar appendage to the O atom for formaldehyde has both been previously reported[13,14] and found in this work.

Additionally, similar structures have been determined through computational methods for large aldehydes,[58] with the O-appended neutral structures seeming universal to carbonyl group-containing molecules. Given that this was the only neutral structure confirmed for the halogen-acetone complexes in this work, and the C-appended formaldehyde neutral complexes being much more computationally unstable, the O-appended structures are of great importance. This importance extends through to atmospheric chemistry, with this type of structure likely being the dominant pre-reaction adduct in the hydrogen abstraction of atmospheric aldehydes and simple ketones. Attempts to converge a C-appended neutral structure for the halogen-acetone complexes were successful, however much like the $F \cdots CH_2O$ complex these stationary points were found to be transition states.

The computational data garnered using the MP2 CBS extrapolation overall provided reasonable estimates of experimental binding energies and E_{stab} values. Calculated EA and E_{stab} numbers underestimated the experimental values by a constant 2-300 meV, while the VDE calculations were inconsistent. An improvement of the optimised geometries to the CCSD(T)/aug-cc-pVTZ level of theory and subsequent energy calculations is the next step for work on the acetone complexes. The CCSD(T) energies should provide a more accurate estimation of the experimental energies.

The chloride, bromide, and iodide formaldehyde complexes all converged to three similar geometries. The anion cluster was found to be a C_{2v} structure with the halide positioned between the two H atoms. The neutral clusters converged to C_s O-appended and C-appended geometries. Trends included an increase in the distance between the halide and formaldehyde as the halide size increased in addition to the widening of angles made with the carbonyl bond for the larger halides. The O-appended structures were consistently found by both MP2 and CCSD(T) calculations to be more stable than those appended to the C atom. This may have atmospheric implications, with the O-appended structures seeming more likely to be the pre-reaction adducts for the hydrogen abstraction of formaldehyde. Additionally, the proposed pre-reaction adduct of Gruber-Stadler et al.[14] was determined to be a transition state upon conducting vibrational analyses.

The fluoride-formaldehyde complexes did not converge similarly to the other halides, barring the universal O-appended structure. The anion complex was appended to a single hydrogen as opposed to two, and attempts to converge the C-appended neutral structure resulted in a transition state being found. This anion complex had the largest D_0 value calculated for the formaldehyde complexes, indicating high stability.

Despite no photoelectron spectra of halide-formaldehyde complexes being taken during this project, the calculations (in particular those converged to the CCSD(T) level) should provide accurate predictions of experimental energies. The same trend observed for the acetone complexes, that E_{stab} decreased with increasing halide size (resulting from anion D_0 values decreasing while neutral D_0 increased) was found true for the formaldehyde complexes, although only computationally. The one exception was between the chloride and fluoride complexes with formaldehyde. As it includes a smaller halide it would be expected that the neutral $F \cdots CH_2O$ would have a smaller D_0 than that of the same O-appended $Cl \cdots CH_2O$ complex. However, the closer distance of the fluoride ion may have led to a higher calculated dissociation energy (15.9 kJ mol^{-1} for $F \cdots CH_2O$ opposed to 15.0 kJ mol^{-1} for $Cl \cdots CH_2O$ using the CCSD(T) extrapolation).

3.2.10 Comparisons to Literature and Other Complexes

Figure 1.3 has been replicated here for ease of comparison between the complexes studied in this work and the geometries obtained for previously studied $Cl^{-}\cdots CO$ and $Cl\cdots CO$ complexes.[33] Firstly, the anion geometries of both formaldehyde and acetone clusters seemed to form H-appended structures. The anion geometry of Figure 3.27 shows a 'tee' structure with the halide situated between the C and O atoms, although appended to the carbon. This is interesting as the work of this project demonstrates the effect of hydrogen additions to the CO molecule on the halide positions. As would be expected, the halides position themselves closer to the C atom due to the induced positive dipole, and indeed even more so closely to the induced dipoles on the H atoms for the formaldehyde and acetone complexes.

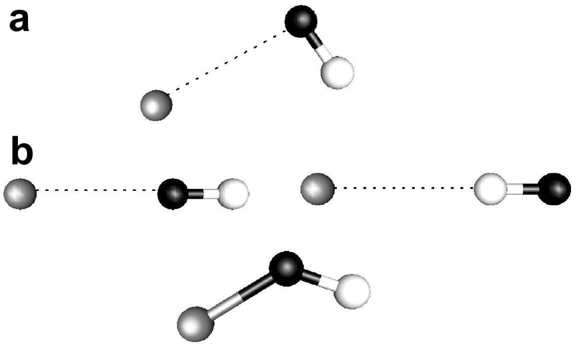

Figure 3.27: Computer structures of (a) $Cl^{-}\cdots CO$ anion, and (b) $Cl\cdots CO$, $Cl\cdots OC$ and ClCO neutral van der Waals clusters.[33]

This work also found an O-appended structure to exist for each neutral complex. This was also observed in the study of $Cl\cdots CO$, with the halogen positioned linearly along the CO axis at both ends of the molecule. These O and C-appended geometries may be similar to those presented in this work, with the hydrogen and methyl groups of formaldehyde and acetone respectively moving the position of the halogen to a new equilibrium point. The ClCO geometry also bears a resemblance to the bent shaped O-appended neutral structures converged for the formaldehyde complexes, with the addition of hydrogens perhaps resulting in the formation of a van der Waals cluster in place of a covalently bonded molecule.

Additionally, the dissociation energies D_0 and E_{stab} values determined experimentally for the chloride-acetone complex and computationally for the chloride-formaldehyde complex were relatively high. Table 3.10 compiles the D_0 and E_{stab} energies of chloride complexes with nitrogen,[59] carbon monoxide,[33] carbon dioxide,[26] and water[29] with those obtained in this work through experiment (acetone) and theory (formaldehyde).

Table 3.10: D_0 and E_{stab} energies of chloride complexes.

Chloride complex	D_0 (kJ mol^{-1})	E_{stab} (eV)
N_2	8.5	0.110
CO	14.6	0.16
CO_2	28.5	0.355
CH_2O	49.6	0.358
C_3H_6O	59.2	0.683
H_2O	61.2	0.760

The values of D_0 were taken from the theoretical calculations of this work. For the formaldehyde complex the E_{stab} value was taken from that calculated for the O-appended neutral structure optimised to the CCSD(T)/aug-cc-pV(T+d)Z level of theory. The acetone E_{stab} is experimental. Some D_0 energies were taken from the NIST Chemistry WebBook.[60] A clear trend is evident in that D_0 values increase with E_{stab}. The energies of the complexes studied in this work are more comparable to the oxygen-containing complexes with clear and apparent dipoles. The greater the dipole, the more strongly bound the complex is, with the chloride-acetone complex found to be almost as tightly bound as the chloride-water complex. Although only computational studies were conducted on the chloride-formaldehyde complex, it would seemingly sit between CO_2 and acetone in terms of binding energies.

4 Conclusion and Future Work

The aims of this project were to investigate the way in which halogens interact with simple carbonyl-containing molecules. Photoelectron spectra of chloride-acetone, bromide-acetone, and iodide-acetone have been recorded and presented in this work for the first time. While no photoelectron spectra were recorded for halide-formaldehyde complexes, CCSD(T) calculations were conducted on these clusters to provide accurate predictions of experimental values.

Through experiment, the binding energy of the chloride-acetone complex was found to be 4.377 eV for the $^2P_{3/2}$ state. The $^2P_{3/2}$ and $^2P_{1/2}$ binding energies of the bromide-acetone and iodide-acetone complexes were determined to be 3.933 eV and 4.393 eV, and 3.511 eV and 4.466 eV respectively. The E_{stab} values, determined through photoelectron spectroscopy as the shifts in binding energy between the bare halide and the complex, ranged from 0.452 eV to 0.683 eV from the halides large to small. This suggests that halide-acetone complexes are very stable relative to the bare halides.

Ab initio calculations were performed to determine geometries and energies of halide-acetone anion and halogen-acetone neutral complexes for experimental comparison. These calculations, conducted to the MP2/aug-cc-pVTZ level, provided reasonable estimates of experimental binding energies and E_{stab} values relative to the computed EA and E_{stab} numbers. However, the VDE calculations were inconsistent. Improving upon these calculations is the next step in an analysis of halogen-acetone interactions. Firstly, testing the VDE calculations with new basis sets and levels of theory will provide more, perhaps even more accurate, comparisons to experiment. Secondly, converging the known MP2 acetone complex geometries at higher levels of theory will allow for the experimental energies to be rationalised and explained with high accuracy.

The halide-acetone anion complexes were all found to converge at a C_s symmetry with the halide positioned out of plane relative to the acetone molecule. The neutral complexes converged to a C_s O-appended structure. Continuing on from previous work conducted in the literature, this O-appended structure seems to be common among all halogen complexes with carbonyl-containing molecules.[13,58]

The halide-formaldehyde anion complexes converged to a C_{2v} structure with the halide postioned in between the two H atoms of formaldehyde (with the exception of $F^{-}\cdots CH_2O$, which converged to a C_s structure appended to one hydrogen). The neutral structures were found to be similarly O-appended or C-appended with both geometries being of C_s symmetry. The computational studies showed that the O-appended structures were more stable with higher D_0 energies, having potential implications for atmospheric interactions. The pre-reaction adduct of the hydrogen abstraction of simple carbonyls likely takes the shape of these O-appended neutral clusters.

The CCSD(T) calculations conducted on the halide-formaldehyde complexes are the highest level calculations completed on these clusters. Future work will entail taking photoelectron spectra of these complexes and comparing the results to the computations described in this work. The new SEVI apparatus to be added to the TOF-PES will allow for these spectra to be taken (or retaken in the case of halide-acetone) in higher resolution.

References

[1] Kritz, M.; Rancher, J. *J. Geophys. Res.* **1980**, *85*, 1633-1639.

[2] Solomon, S. *Nature.* **1991**, *347*, 347-353.

[3] Wayne, R.P.; *Chemistry of Atmospheres*, 3rd ed.; Oxford University Press: New York, 2000.

[4] Singh, H. B.; OHara, D.; Herlth, D.; Sachse, W.; Blake, D. R.; Bradshaw, J. D.; Kanakidou, M.; Crutzen, P. J. *J. Geophys. Res.* **1994**, *99*, 1805-1819.

[5] Nielsen, O. J.; Johnson, M. S.; Wallington, T. J.; Christensen, L. K.; Platz, J. *Int. J. Chem. Kinet.* **2002**, *34*, 283-291.

[6] Tiu, G. C.; Tao, F. *Chem. Phys. Lett.* **2006**, *428*, 42-48.

[7] Carr, S.; Shallcross, D. E.; Canosa-Mas, C. E.; Wenger, J.C.; Sidebottom, H. W.; Treacy, J. J.; Wayne, R. P. *Phys. Chem. Chem. Phys.* **2003**, *5*, 3874- 3883.

[8] Zhang, H.; Zhang, G.; Liu, J.; Sun, M.; Liu, B.; Li, Z. *Theor. Chem. Acc.* **2011**, *128*, 317-325.

[9] Li, Y.; Li, H.; Hou, H.; Wang, B. *J. Phys. Chem. A.* **2005**, *109*, 3166-3173.

[10] Feilberg, K. L.; Johnson, M. S.; Nielsen, C. J. *J. Phys. Chem. A.* **2004**, *108*, 7393-7398.

[11] Shepson, P. B.; Sirju, A.-P.; Hopper, J. R.; Barrie, L. A.; Young, V.; Niki, H.; Dryfhout, H. *J. Geophys. Res.* **1996**, *101*, 21081-21089.

[12] Barrie, L. A.; Bottenheim, J. W.; Schnell, R. C.; Crutzen, P. J.; Rasmussen, R. A. *Nature.* **1988**, *334*, 138-141.

[13] Beukes, J. A.; Danna, B.; Bakken, V.; Nielsen, C. *J. Phys. Chem. Chem. Phys.* **2000**, *2*, 4049-4060.

[14] Gruber-Stadler, M.; Muhlhauser, M.; Sellevag, S. R.; Nielsen, C. J. *J. Phys. Chem. A*. **2008**, *112*, 9-22.

[15] Walsh, R.; Benson, S. W. *J. Am. Chem. Soc.* **1966**, *88*, 4570-4575.

[16] Muller-Dethlefs, K.; Hobza, *P. Chem. Rev.* **2000**, *100*, 143-67.

[17] Blaney, B. L.; Ewing, G. E.; *Ann. Rev. Phys. Chem.* **1967**, *271*, 553-584.

[18] Wild, D. A. Infrared Spectroscopy of Size Selected Anion Complexes and Clusters. Ph.D. Thesis, The University of Melbourne, March 2003.

[19] Takashima, K.; Riveros, J. M. *Mass. Spec. Rev.* **1998**, *17*, 409-430.

[20] Lapere, K. M. L. Anion Photoelectron Spectroscopy of Halide Complexes and Clusters. Ph.D. Thesis, The University of Western Australia, August 2014.

[21] Depuy, C. H. Int. *J. Mass. Spec.* **2000**, *200*, 79-96.

[22] Brehm, B.; Gusinow, M. A.; Hall, J. L. Brehm, J. L. *Phys. Rev. Lett.* **1967**, *19*, 737-741.

[23] Watson, P. Anion Photoelectron Spectroscopy and Ab Initio Calculations of Asymmetric Halogen Dioxides. Honours Thesis, The University of Western Australia, May 2015.

[24] Vogelhuber, K. M.; Wren, S. W.; Sheps, L.; Lineberger, W. C. *J. Chem. Phys.* **2011**, *134*, 064302.

[25] Kasdan, A.; Herbst, E.; Lineberger, W. C. *J. Chem. Phys.* **1975**, *62*, 541-548.

[26] Arnold, D. W.; Bradforth, S. E.; Kim, E. H., Neumark, D. M. *J. Chem. Phys.*, **1995**, *102*, 3493-3509.

[27] Wang, X.-B.; Kowalski, K.; Wang, L.-S.; Xantheas, S. S. *J. Chem. Phys.* **2010**, *132*, 124306.

[28] Markovich, G.; Giniger, R.; Levin, M.; Cheshnovsky, O. *J. Chem. Phys.* **1991**, *95*, 9416-9419.

[29] Markovich, G.; Pollack, S.; Giniger, R.; Cheshnovsky, O. *J. Chem. Phys.* **1994**, *101*, 9344-9353.

[30] Neumark, D. M. *Acc. Chem. Res.* **1993**, *26*, 33-39.

[31] Beckham, D. A. R.; Conran, S.; Lapere, K. M.; Kettner, M.; McKinley, A. J.; Wild, D. A. *Chem. Phys. Lett.* **2015**, *619*, 241-246.

[32] Lapere, K. M. L.; Kettner, M.; Watson, P. D.; McKinley, A. J.; Wild, D. A. *J. Phys. Chem. A.* **2015**, *119*, 9722-9728.

[33] Lapere, K. M.; LaMacchia, R. J.; Quak, L. H.; McKinley, A. J.; Wild, D. A. *Chem. Phys. Lett.* **2011**, *504*, 13-19.

[34] Lapere, K. M.; LaMacchia, R. J.; Quak, L. H.; Kettner, M.; Dale, S. G.; McKinley, A. J.; Wild, D. A. *Aust. J. Chem.* **2012**, *65*, 457-462.

[35] Lapere, K. M.; LaMacchia, R. J.; Quak, L. H.; Kettner, M. K.; Dale, S. G.; McKinley, A. J.; Wild, D. A. *J. Phys. Chem. A.* **2012**, *116*, 3577-3584.

[36] Sadlej, J.; Szczesniak, M. M.; Chalasinski, G. *J. Chem. Phys.* **1993**, *99*, 5211-5218.

[37] Lewars, E. G. *Computational Chemistry: Introduction to the Theory and Applications of Molecular and Quantum Mechanics*, 2nd Ed.; Springer Netherlands: Dordrecht, 2011.

[38] Hinchcliffe, A. *Computational Quantum Chemistry*; John Wiley and Sons: Chichester, U.K., 1988.

[39] Jung, Y.; Lochan, R. C.; Dutoi, A. D.; Head-Gordon, M. *J. Chem. Phys.* **2004**, *121*, 9793-9802.

[40] Hasanein, A. A.; Evans, M. W. *Computational Methods in Quantum Chemistry: Quantum Chemistry Vol. 2*; World Scientific Publishing: Singapore, 1996.

[41] Bartlett, R. J.; Musial, M. *Rev. Mod. Phys.* **2007**, *79*, 291-352.

[42] Wiley, W. C.; McLaren, I. H. *Rev. Sci. Intsrum.* **1955**, *26*, 1150-1157.

[43] LaMacchia, R.J. Towards Anion Photoelectron Spectroscopy of Complexes and Clusters. Honours Thesis, The University of Western Australia, November 2008.

[44] *Negative Ion Energetics Data*; P. J. Linstrom, W. G. Mallard, Eds.; NIST Chemistry WebBook, NIST Standard Reference Database; National Institute of Standards and Technology: Gaithersburg MD, 20899.

[45] Frisch, M. J.; Trucks, G. W.; Schlegel, H. B.; Scuseria, G. E.; Robb, M. A.; Cheeseman, J. R.; Scalmani, G.; Barone, V.; Mennucci, B.; Petersson, G. A.; Nakatsuji, H.; Caricato, M.; Li, X.; Hratchian, H. P.; Izmaylov, A. F.; Bloino, J.; Zheng, G.; Sonnenberg, J. L.; Hada, M.; Ehara, M.; Toyota, K.; Fukuda, R.; Hasegawa, J.; Ishida, M.; Nakajima, T.; Honda, Y.; Kitao, O.; Nakai, H.; Vreven, T.; Montgomery Jr., J. A.; Peralta, J. E.; Ogliaro, F.; Bearpark, M.; Heyd, J. J.; Brothers, E.; Kudin, K. N.; Staroverov, V. N.; Kobayashi, R.; Normand, J.; Raghavachari, K.; Rendell, A.; Burant, J. C.; Iyengar, S. S.; Tomasi, J.; Cossi, M.; Rega, N.; Millam, J. M.; Klene, M.; Knox, J. E.; Cross, J. B.; Bakken, V.; Adamo, C.; Jaramillo, J.; Gomperts, R.; Stratmann, R. E.; Yazyev, O.; Austin, A. J.; Cammi, R.; Pomelli, C.; Ochterski, J. W.; Martin, R. L.; Morokuma, K.; Zakrzewski, V. G.; Voth, G. A.; Salvador, P.; Dannenberg, J. J.; Dapprich, S.; Daniels, A. D.; Farkas, Ö.; Foresman, J. B.; Ortiz, J. V.; Cioslowski, J.; Fox, D. J. Gaussian 09 Revision A.01.

[46] Stanton, J. F.; Gauss, J.; Harding, M. E.; Szalay, P. G. CFOUR, Coupled-Cluster Techniques for Computational Chemistry.

[47] Dunning, Jr., T. H. *J. Chem. Phys.* **1989**, *90*, 1007-1023.

[48] Kendall, R. A.; Dunning, Jr., T. H.; Harrison, R. J. *J. Chem. Phys.* **1992**, *96*, 6796-6806.

[49] Woon, D. E.; Dunning, Jr., T. H. *J. Chem. Phys.* **1993**, *98*, 1358-1371.

[50] Dunning, Jr., T. H.; Peterson, K. A.; Wilson, A. K. *J. Chem. Phys.* **2001**, *114*, 9244-9253.

[51] Peterson, K. A.; Figgen, D.; Goll, E.; Stoll, H.; Dolg, M. *J. Chem. Phys.* **2003**, *119*, 11113.

[52] Peterson, K. A.; Shepler, B. C.; Figgen, D.; Stoll, H. *J. Phys. Chem. A* **2006**, *110*, 13877.

[53] Schuchardt, K. L.; Didier, B. T.; Elsethagen, T.; Sun, L.; Gurumoorthi, V.; Chase, J.; Li, J.; Windus, T. L. *J. Chem. Inf. Model.* **2007**, *47*, 10451052.

[54] Karton, A.; Martin, J. M. L. *Theor. Chem. Acc.* **2006**, *115*, 330-333.

[55] Kettner, M. Aspects of Gas-Phase Anion Spectroscopy. Ph.D Thesis, The University of Western Australia, September 2015.

[56] Neese, F.; Valeev, E.F. *J. Chem. Theory Comput.* **2011**, *7*, 33-43.

[57] Panich, A. M. *Chem. Phys.* **1995**, *196*, 511-519.

[58] Srinivasulu, G.; Rajakumar, B. *J. Chem. Sci.* **2016**, *128*, 977-989.

[59] Watson, P. D.; Yong, H.-W.; Lapere, K. M. L,; Kettner, M.; McKinley, A. J.; Wild, D. A. *Chem. Phys. Lett.* **2016**, *654*, 119-124.

[60] *Binding Energies Between Ions and Molecules, and the Thermochemistry of Cluster Ions*; P. J. Linstrom, W. G. Mallard, Eds.; NIST Chemistry WebBook, National Institute of Standards and Technology: Gaithersburg MD, 20899.

A Data and Tables

Table A.1: Energies and geometries of the acetone molecule.

MP2	E_h Hartree	zpe kJ mol^{-1}	$r_{\mathrm{C=O}}$ Å	$r_{\mathrm{C-C}}$ Å	$r_{\mathrm{C-H}}$ Å	$\angle_{O\text{-}C\text{-}C}$ °
TZ	-192.7901427	221.17	1.220	1.509	1.086/1.091	121.9
QZ	-192.8452889					
CBS	-192.8788538					

Table A.2: Energies and geometries of the formaldehyde molecule.

MP2	E_h Hartree	zpe kJ mol^{-1}	$r_{\mathrm{C=O}}$ Å	$r_{\mathrm{C-H}}$ Å	$\angle_{O\text{-}C\text{-}H}$ °
TZ	-114.3164101	70.44	1.213	1.100	121.7
QZ	-114.3486469				
5Z	-114.3602853				
CBS	-114.3715272				
CCSD(T)					
TZ	-114.3429335	69.80	1.212	1.103	121.7
QZ	-114.3723566				
5Z	-114.3815939				
CBS	-114.3903166				

Table A.3: Vibrational frequencies and intensities of acetone at the MP2/aug-cc-pVTZ level.

Vibrational frequency (cm^{-1})	Intensity ($km\ mol^{-1}$)
23	0.0
141	0.1
377	1.3
484	0.5
531	14.4
806	1.64
892	0.0
902	5.3
1087	0.0
1121	1.6
1254	52.9
1392	14.9
1400	64.3
1478	0.4
1485	0.0
1486	31.4
1509	19.5
1756	130.2
3070	0.8
3075	5.3
3149	0.0
3155	10.1
3200	7.6
3201	2.9

Table A.4: Vibrational frequencies and intensities of formaldehyde at the MP2/aug-cc-pVTZ and CCSD(T)/aug-cc-pVTZ levels. Note that the CCSD(T) calculations were run using Gaussian 09, which cannot calculate intensities at this level.

Vibrational frequency (cm^{-1})		Intensity ($\mathrm{km\ mol}^{-1}$)	
MP2	CCSD(T)	MP2	CCSD(T)
1197	1181	7.0	0.0
1267	1261	9.4	0.0
1540	1529	10.7	0.0
1753	1765	67.8	0.0
2973	2932	66.7	0.0
3048	3000	88.4	0.0

Table A.5: Structural parameters of the halide-acetone anion complexes at the MP2/aug-cc-pVTZ (and related custom basis sets) level. Unless stated otherwise, the C · · · X distance is to the central C atom of acetone while the H · · · X distance is to the nearest hydrogen(s).

Complex	Point group	$r_{\mathrm{C}\cdots\mathrm{X}}$ Å	$r_{\mathrm{O}\cdots\mathrm{X}}$ Å	$r_{\mathrm{H}\cdots\mathrm{X}}$ Å	$\angle_{O\text{-}C\text{-}X}$ °
$F^{-}\cdots C_3H_6O$	C_s	3.263	4.313	1.902	143.4
$C^{-}\cdots C_3H_6O$	C_s	3.914	4.961	2.515	144.1
$Br^{-}\cdots C_3H_6O$	C_s	4.045	5.095	2.628	144.6
$I^{-}\cdots C_3H_6O$	C_s	4.313	5.367	2.877	145.3

Table A.6: Energies calculated for the halide-acetone anion complexes.

			MP2 E_h (Hartree)		
Complex	zpe (kJ mol^{-1})	Corrected zpe (kJ mol^{-1})	TZ	QZ	CBS
$F^{-}\cdots C_3H_6O$	222.78	2.42	-292.5714046	-292.6549383	-292.7055590
$Cl^{-}\cdots C_3H_6O$	223.54	1.78	-652.5944296	-652.6715071	-652.7193590
$Br^{-}\cdots C_3H_6O$	223.07	1.66	-608.6318528	-608.7652795	-608.8540360
$I^{-}\cdots C_3H_6O$	223.68	1.43	-487.7769697	-487.9126813	-488.0034540

Table A.7: Vibrational frequencies and intensities for the fluoride and chloride acetone complexes at the MP2/aug-cc-pVTZ and aug-cc-pV(T+d)Z levels respectively.

$F^{-}\cdots C_3H_6O$		$Cl^{-}\cdots C_3H_6O$	
Vibrational frequency (cm^{-1})	Intensity ($km\ mol^{-1}$)	Vibrational frequency (cm^{-1})	Intensity ($km\ mol^{-1}$)
78	13.1	57	7.6
117	22.6	112	7.3
210	87.1	130	36.2
233	2.0	162	1.2
286	0.0	222	1.0
410	24.9	392	11.9
514	11.4	501	3.7
526	9.6	530	10.5
823	3.2	818	2.5
897	3.5	895	1.5
935	3.3	926	5.4
1108	4.5	1101	2.2
1128	8.2	1126	4.2
1248	23.4	1259	30.3
1405	10.5	1400	5.4
1410	96.5	1412	58.0
1456	1.6	1469	0.3
1491	9.1	1483	2.6
1494	1.3	1487	54.2
1511	84.7	1504	26.2
1725	201.2	1733	190.2
2852	64.8	2999	28.9
2890	506.8	3007	238.7
3083	6.1	3105	0.4
3090	31.4	3111	45.8
3162	36.1	3175	24.7
3165	21.2	3177	10.6

Table A.8: Vibrational frequencies and intensities for the bromide and iodide acetone complexes at the MP2/aug-cc-pVTZ PP level.

$Br^{-}\cdots C_3H_6O$		$I^{-}\cdots C_3H_6O$	
Vibrational frequency (cm^{-1})	Intensity ($km\ mol^{-1}$)	Vibrational frequency (cm^{-1})	Intensity ($km\ mol^{-1}$)
53	4.2	46	3.7
111	15.5	91	8.9
114	3.2	101	2.0
162	0.7	140	0.6
222	0.7	203	0.9
392	10.8	388	9.0
501	3.9	497	2.9
530	10.2	531	10.2
818	2.7	817	2.8
894	1.3	893	0.7
926	5.8	922	6.5
1101	2.1	1099	1.8
1126	4.0	1123	2.9
1259	29.0	1260	28.3
1401	4.5	1399	4.7
1413	51.0	1411	43.3
1471	0.2	1471	0.0
1482	2.7	1479	2.7
1486	63.0	1484	73.3
1505	22.4	1502	16.3
1734	194.9	1725	195.9
3005	28.2	3020	21.3
3011	237.3	3024	182.6
3107	0.2	3113	0.0
3113	46.8	3118	44.9
3177	23.0	3180	20.5
3179	8.7	3182	5.8

Table A.9: Structural parameters of the halogen-acetone neutral complexes at the MP2/aug-cc-pVTZ (and related custom basis sets) level. Unless stated otherwise, the C $\cdots$ X distance is to the central C atom of acetone while the H $\cdots$ X distance is to the nearest hydrogen(s).

Complex	Point group	$r_{\mathrm{C}\cdots\mathrm{X}}$ Å	$r_{\mathrm{O}\cdots\mathrm{X}}$ Å	$r_{\mathrm{H}\cdots\mathrm{X}}$ Å	$\angle_{C\text{-}O\text{-}X}$ °
F $\cdots$ C_3H_6O	C_s	3.161	2.367	2.551	120.1
Cl $\cdots$ C_3H_6O	C_s	3.320	2.510	2.730	121.6
Br $\cdots$ C_3H_6O	C_s	3.433	2.621	2.785	122.1
I $\cdots$ C_3H_6O	C_s	3.667	2.833	2.991	124.3

Table A.10: Energies calculated for the halogen-acetone neutral complexes.

			MP2 E_h (Hartree)		
Complex	zpe (kJ mol^{-1})	Corrected zpe (kJ mol^{-1})	TZ	QZ	CBS
F $\cdots$ C_3H_6O	222.82	0.86	-292.4059843	-292.4869306	-292.5354823
Cl $\cdots$ C_3H_6O	221.90	1.23	-652.4458693	-652.5194716	-652.5646965
Br $\cdots$ C_3H_6O	223.38	1.17	-608.4918530	-608.6225160	-608.7091805
I $\cdots$ C_3H_6O	222.95	1.01	-487.6463652	-487.7788608	-488.8672193

Table A.11: Vibrational frequencies and intensities for the fluorine and chlorine neutral acetone complexes at the MP2/aug-cc-pVTZ and aug-cc-pV(T+d)Z levels respectively.

$F \cdots C_3H_6O$		$Cl \cdots C_3H_6O$	
Vibrational frequency (cm^{-1})	Intensity ($km\ mol^{-1}$)	Vibrational frequency (cm^{-1})	Intensity ($km\ mol^{-1}$)
29	2.8	34	2.0
36	0.0	70	0.5
79	0.3	103	4.3
106	7.6	127	3.4
137	0.1	140	16.9
381	2.2	385	4.0
485	0.5	485	0.6
540	17.8	548	21.8
809	1.1	812	0.6
894	0.0	895	0.2
907	4.4	917	3.6
1090	0.0	1091	0.1
1122	1.9	1122	2.2
1259	46.7	1262	31.5
1393	14.9	1393	11.1
1402	61.1	1403	55.6
1478	0.7	1477	4.0
1484	18.4	1480	26.5
1487	14.6	1488	9.2
1510	19.0	1508	17.2
1758	173.8	1759	281.2
3072	0.4	3072	0.0
3076	6.2	3076	6.2
3150	0.3	3152	1.4
3156	8.3	3158	5.1
3202	4.8	3205	3.6
3210	2.1	3211	0.8

Table A.12: Vibrational frequencies and intensities for the bromine and iodine neutral acetone complexes at the MP2/aug-cc-pVTZ PP level.

$Br \cdots C_3H_6O$		$I \cdots C_3H_6O$	
Vibrational frequency (cm^{-1})	Intensity (km mol^{-1})	Vibrational frequency (cm^{-1})	Intensity (km mol^l-1)
40	2.5	33	2.6
61	0.1	55	0.1
93	2.2	81	1.4
126	10.1	109	12.5
132	5.2	130	0.2
386	3.9	385	3.7
487	0.5	487	0.4
548	20.5	543	19.5
814	0.6	813	0.7
895	0.2	894	0.2
915	3.4	914	3.3
1092	0.1	1091	0.1
1123	1.9	1123	1.7
1264	32.7	1263	37.3
1393	13.8	1394	16.5
1403	55.9	1403	55.8
1476	2.9	1476	1.7
1480	25.0	1480	22.5
1487	9.5	1486	10.9
1508	16.2	1507	15.2
1755	261.4	1749	235.5
3072	0.3	3070	0.8
3076	6.4	3075	5.7
3152	1.0	3151	0.9
3157	4.9	3157	4.9
3205	3.7	3200	1.5
3207	0.7	3204	3.2

Table A.13: Structural parameters of the halide-formaldehyde complexes at the MP2/aug-cc-pVTZ (and related custom basis sets) level.

Complex	Point group	$r_{\mathrm{C\cdots X}}$ Å	$r_{\mathrm{O\cdots X}}$ Å	$r_{\mathrm{H\cdots X}}$ Å	$\angle_{O\text{-}C\text{-}X}$ °
$F^{-}\cdots CH_2O$	C_s	2.769	3.760	1.673	136.8
$Cl^{-}\cdots CH_2O$	C_{2v}	3.256	4.479	2.813	180.0
$Br^{-}\cdots CH_2O$	C_{2v}	3.390	4.612	2.940	180.0
$I^{-}\cdots CH_2O$	C_{2v}	3.636	4.857	3.177	180.0

Table A.14: Structural parameters of the halide-formaldehyde complexes at the CCSD(T)/aug-cc-pVTZ (and related custom basis sets) level.

Complex	Point group	$r_{\mathrm{C\cdots X}}$ Å	$r_{\mathrm{O\cdots X}}$ Å	$r_{\mathrm{H\cdots X}}$ Å	$\angle_{O\text{-}C\text{-}X}$ °
$F^{-}\cdots CH_2O$	C_s	2.758	3.750	1.659	136.9
$Cl^{-}\cdots CH_2O$	C_{2v}	3.262	4.484	2.817	180.0
$Br^{-}\cdots CH_2O$	C_{2v}	3.403	4.624	2.951	180.0
$I^{-}\cdots CH_2O$	C_{2v}	3.650	4.869	3.189	180.0

Table A.15: Energies calculated for the halide-formaldehyde anion complexes at both MP2 and CCSD(T) levels.

			MP2 E_h (Hartree)			
Complex	zpe (kJ mol^{-1})	Corrected zpe (kJ mol^{-1})	TZ	QZ	5Z	CBS
$F^{-}\cdots CH_2O$	72.01	4.15	-214.0917407	-214.1524400	-214.1750302	-214.1967784
$Cl^{-}\cdots CH_2O$	71.98	1.38	-574.1173780	-574.1711172	-574.1912518	-574.2111702
$Br^{-}\cdots CH_2O$	71.79	1.24	-530.1533305	-530.2643344	-530.3630139	-530.4655449
$I^{-}\cdots CH_2O$	71.78	1.24	-409.2991739	-409.4120580	-409.4838965	-409.5582931
			CCSD(T) E_h (Hartree)			
$F^{-}\cdots CH_2O$	71.40	4.22	-214.1231468	-214.1799244	-214.1984008	-214.2158334
$Cl^{-}\cdots CH_2O$	71.36	1.41	-574.1690691	-574.2190533	-574.2353018	-574.2511421
$Br^{-}\cdots CH_2O$	71.11	1.20	-530.1979291	-530.3034144	-530.3911681	-530.4822361
$I^{-}\cdots CH_2O$	71.10	1.24	-409.3419803	-409.4503782	-409.5149521	-409.5817269

Table A.16: Vibrational frequencies and intensities for the fluoride-formaldehyde anion complex at the MP2/aug-cc-pVTZ and CCSD(T)/aug-cc-pVTZ levels.

Vibrational frequency (cm^{-1})		Intensity ($\mathrm{km\ mol}^{-1}$)	
MP2	CCSD(T)	MP2	CCSD(T)
148	148	17.0	0.0
253	259	105.9	0.0
292	297	11.6	0.0
1243	1236	126.3	0.0
1321	1310	5.8	0.0
1539	1530	142.1	0.0
1714	1717	91.8	0.0
2647	2611	571.6	0.0
2883	2830	238.9	0.0

Table A.17: Vibrational frequencies and intensities for the chloride-formaldehyde anion complex at the MP2/aug-cc-pV(T+d)Z and CCSD(T)/aug-cc-pV(T+d)Z levels.

Vibrational frequency (cm^{-1})		Intensity ($\mathrm{km\ mol}^{-1}$)	
MP2	CCSD(T)	MP2	CCSD(T)
37	43	26.0	26.0
67	66	17.4	17.4
127	127	18.2	18.4
1200	1195	4.8	5.7
1240	1226	4.8	4.3
1497	1486	93.0	99.6
1725	1733	84.3	94.8
3022	2983	25.8	22.6
3119	3072	31.3	34.4

Table A.18: Vibrational frequencies and intensities for the bromide-formaldehyde anion complex at the MP2/aug-cc-pVTZ PP and CCSD(T)/aug-cc-pVTZ PP levels.

Vibrational frequency (cm^{-1})		Intensity (km mol^{-1})	
MP2	CCSD(T)	MP2	CCSD(T)
39	46	21.4	0.0
63	49	14.1	0.0
105	105	5.0	0.0
1204	1198	3.5	0.0
1237	1223	4.234	0.0
1500	1489	95.7	0.0
1727	1736	85.0	0.0
3015	2976	30.3	0.0
3111	3065	28.8	0.0

Table A.19: Vibrational frequencies and intensities for the iodide-formaldehyde anion complex at the MP2/aug-cc-pVTZ PP and CCSD(T)/aug-cc-pVTZ PP levels.

Vibrational frequency (cm^{-1})		Intensity (km mol^{-1})	
MP2	CCSD(T)	MP2	CCSD(T)
41	47	19.4	0.0
76	63	13.1	0.0
91	90	1.9	0.0
1216	1210	2.5	0.0
1233	1219	3.6	0.0
1507	1496	95.5	0.0
1731	1740	85.8	0.0
3004	2966	37.9	0.0
3102	3056	26.6	0.0

Table A.20: Structural parameters of the C-appended halogen-formaldehyde neutral complexes at the MP2)/aug-cc-pVTZ (and related custom basis sets) level.

Complex	Point group	$r_{\mathrm{C}\cdots\mathrm{X}}$ Å	$r_{\mathrm{O}\cdots\mathrm{X}}$ Å	$r_{\mathrm{H}\cdots\mathrm{X}}$ Å	$\angle_{O\text{-}C\text{-}X}$ °
$\mathrm{Cl}\cdots\mathrm{CH_2O}$	C_s	3.482	4.284	3.325	124.3
$\mathrm{Br}\cdots\mathrm{CH_2O}$	C_s	3.510	4.288	3.366	122.7
$\mathrm{I}\cdots\mathrm{CH_2O}$	C_s	3.683	4.473	3.514	123.8

Table A.21: Structural parameters of the O-appended halogen-formaldehyde neutral complexes at the MP2/aug-cc-pVTZ (and related custom basis sets) level.

Complex	Point group	$r_{\mathrm{C}\cdots\mathrm{X}}$ Å	$r_{\mathrm{O}\cdots\mathrm{X}}$ Å	$r_{\mathrm{H}\cdots\mathrm{X}}$ Å	$\angle_{C\text{-}O\text{-}X}$ °
$\mathrm{F}\cdots\mathrm{CH_2O}$	C_s	2.951	2.443	2.730	102.4
$\mathrm{Cl}\cdots\mathrm{CH_2O}$	C_s	3.183	2.621	2.981	106.5
$\mathrm{Br}\cdots\mathrm{CH_2O}$	C_s	3.275	2.714	3.058	106.7
$\mathrm{I}\cdots\mathrm{CH_2O}$	C_s	3.488	2.928	3.244	107.4

Table A.22: Structural parameters of the halogen-formaldehyde neutral complexes at the CCSD(T)/aug-cc-pVTZ (and related custom basis sets) level.

Complex	Point group	$r_{\mathrm{C}\cdots\mathrm{X}}$ Å	$r_{\mathrm{O}\cdots\mathrm{X}}$ Å	$r_{\mathrm{H}\cdots\mathrm{X}}$ Å	$\angle_{C\text{-}O\text{-}X}$ °
$\mathrm{F}\cdots\mathrm{CH_2O}$	C_s	2.555	2.040	2.396	100.3
$\mathrm{Cl}\cdots\mathrm{CH_2O}$	C_s	3.118	2.550	2.925	106.3
$\mathrm{Br}\cdots\mathrm{CH_2O}$	C_s	3.255	2.684	3.046	107.0
$\mathrm{I}\cdots\mathrm{CH_2O}$	C_s	3.494	2.925	3.257	107.8

Table A.23: Energies of the C-appended halogen-formaldehyde complexes at the MP2 and CCSD(T) levels of theory using the MP2 geometries.

			MP2 E_h (Hartree)			
Complex	zpe (kJ mol^{-1})	Corrected zpe (kJ mol^{-1})	TZ	QZ	5Z	CBS
$\mathrm{Cl} \cdots \mathrm{CH_2O}$	71.92	1.55	-573.9658358	-574.0163111	-574.0350703	-574.0535028
$\mathrm{Br} \cdots \mathrm{CH_2O}$	72.02	1.69	-530.0102973	-530.1177292	-530.2150110	-530.3160303
$\mathrm{I} \cdots \mathrm{CH_2O}$	72.06	1.77	-409.1649015	-409.2738045	-409.3438800	-409.4163669
			CCSD(T) E_h (Hartree)			
$\mathrm{Cl} \cdots \mathrm{CH_2O}$	-	-	-574.0221770	-574.0695541	-574.0841719	-574.0982593
$\mathrm{Br} \cdots \mathrm{CH_2O}$	-	-	-530.0582092	-530.1597715	-530.2465036	-530.3364544
$\mathrm{I} \cdots \mathrm{CH_2O}$	-	-	-409.2107100	-409.3148009	-	-409.3850874

Table A.24: Energies of the O-appended halogen-formaldehyde complexes at the MP2 and CCSD(T) levels of theory.

			MP2 E_h (Hartree)			
Complex	zpe (kJ mol^{-1})	Corrected zpe (kJ mol^{-1})	TZ	QZ	5Z	CBS
$\mathrm{F} \cdots \mathrm{CH_2O}$	74.63	1.96	-213.9538814	-214.0065997	-214.0237297	-214.0396699
$\mathrm{Cl} \cdots \mathrm{CH_2O}$	76.23	2.53	-573.9700162	-574.0207414	-574.0396182	-574.0581721
$\mathrm{B}\cdots\mathrm{CH_2O}$	76.00	2.55	-530.0151935	-530.1228964	-530.2200858	-530.3210026
$\mathrm{I} \cdots \mathrm{CH_2O}$	75.14	2.41	-409.1696405	-409.2789270	-409.3490336	-409.4215449
			CCSD(T) E_h (Hartree)			
$\mathrm{F} \cdots \mathrm{CH_2O}$	75.18	4.81	-213.9732994	-214.0335291	-214.0514162	-214.0681508
$\mathrm{Cl} \cdots \mathrm{CH_2O}$	73.50	3.16	-574.0273702	-574.0751510	-574.0899200	-574.1041672
$\mathrm{Br} \cdots \mathrm{CH_2O}$	73.06	2.78	-530.0636581	-530.1655439	-530.2522092	-530.3420864
$\mathrm{I} \cdots \mathrm{CH_2O}$	72.65	2.45	-409.2155545	-409.3200267	-409.3832933	-409.4486294

Table A.25: Vibrational frequencies and intensities of the C-appended chlorine-formaldehyde neutral complex at the MP2/aug-cc-pV(T+d)Z level.

Vibrational frequency (cm^{-1})	Intensity ($km\ mol^{-1}$)
24	7.2
72	10.3
163	1.2
1193	6.5
1262	9.4
1538	10.4
1759	74.8
2972	75.4
3042	87.0

Table A.26: Vibrational frequencies and intensities of the C-appended bromine-formaldehyde neutral complex at the MP2/aug-cc-pVTZ PP level.

Vibrational frequency (cm^{-1})	Intensity ($km\ mol^{-1}$)
26	5.6
78	11.1
179	0.9
1189	6.0
1260	9.1
1537	10.5
1762	77.8
2971	77.7
3039	84.5

Table A.27: Vibrational frequencies and intensities of the C-appended iodine-formaldehyde neutral complex at the MP2/aug-cc-pVTZ PP level.

Vibrational frequency (cm^{-1})	Intensity ($km\ mol^{-1}$)
26	5.2
84	12.4
185	0.7
1186	6.0
1259	8.3
1536	11.2
1764	80.5
2969	80.9
3039	77.6

Table A.28: Vibrational frequencies and intensities for the O-appended fluorine-formaldehyde neutral complex at the MP2/aug-cc-pVTZ and CCSD(T)/aug-cc-pVTZ levels.

Vibrational frequency (cm^{-1})		Intensity ($km\ mol^{-1}$)	
MP2	CCSD(T)	MP2	CCSD(T)
91	210	2.1	0.0
117	286	23.3	0.0
120	309	0.5	0.0
1214	1184	6.2	0.0
1270	1237	8.5	0.0
1548	1492	11.5	0.0
2065	1790	461.9	0.0
2995	2983	163.8	0.0
3057	3077	74.0	0.0

Table A.29: Vibrational frequencies and intensities for the O-appended chlorine-formaldehyde neutral complex at the MP2/aug-cc-pV(T+d)Z and CCSD(T)/aug-cc-pV(T+d)Z levels.

Vibrational frequency (cm^{-1})		Intensity ($km\ mol^{-1}$)	
MP2	CCSD(T)	MP2	CCSD(T)
105	123	1.9	0.0
154	188	47.0	0.0
163	217	0.4	0.0
1231	1188	5.2	0.0
1270	1257	5.3	0.0
1545	1517	15.3	0.0
2194	1786	753.2	0.0
3014	2965	260.6	0.0
3068	3048	53.0	0.0

Table A.30: Vibrational frequencies and intensities for the O-appended bromine-formaldehyde neutral complex at the MP2/aug-cc-pVTZ PP and CCSD(T)/aug-cc-pVTZ PP levels.

Vibrational frequency (cm^{-1})		Intensity ($km\ mol^{-1}$)	
MP2	CCSD(T)	MP2	CCSD(T)
102	103	0.8	0.0
153	155	46.3	0.0
171	207	0.4	0.0
1231	1190	5.2	0.0
1269	1256	5.0	0.0
1543	1518	17.6	0.0
2153	1781	659.0	0.0
3013	2961	225.6	0.0
3071	3044	51.8	0.0

Table A.31: Vibrational frequencies and intensities for the O-appended iodine-formaldehyde neutral complex at the MP2/aug-cc-pVTZ PP and CCSD(T)/aug-cc-pVTZ PP levels.

Vibrational frequency (cm^{-1})		Intensity ($km\ mol^{-1}$)	
MP2	CCSD(T)	MP2	CCSD(T)
94	88	0.9	0.0
139	130	43.0	0.0
170	193	0.4	0.0
1223	1191	5.2	0.0
1269	1260	5.0	0.0
1543	1522	21.1	0.0
2049	1771	441,7	0.0
3004	2956	154.9	0.0
3072	3036	57.5	0.0

B Diagram of TOF-PES Timing

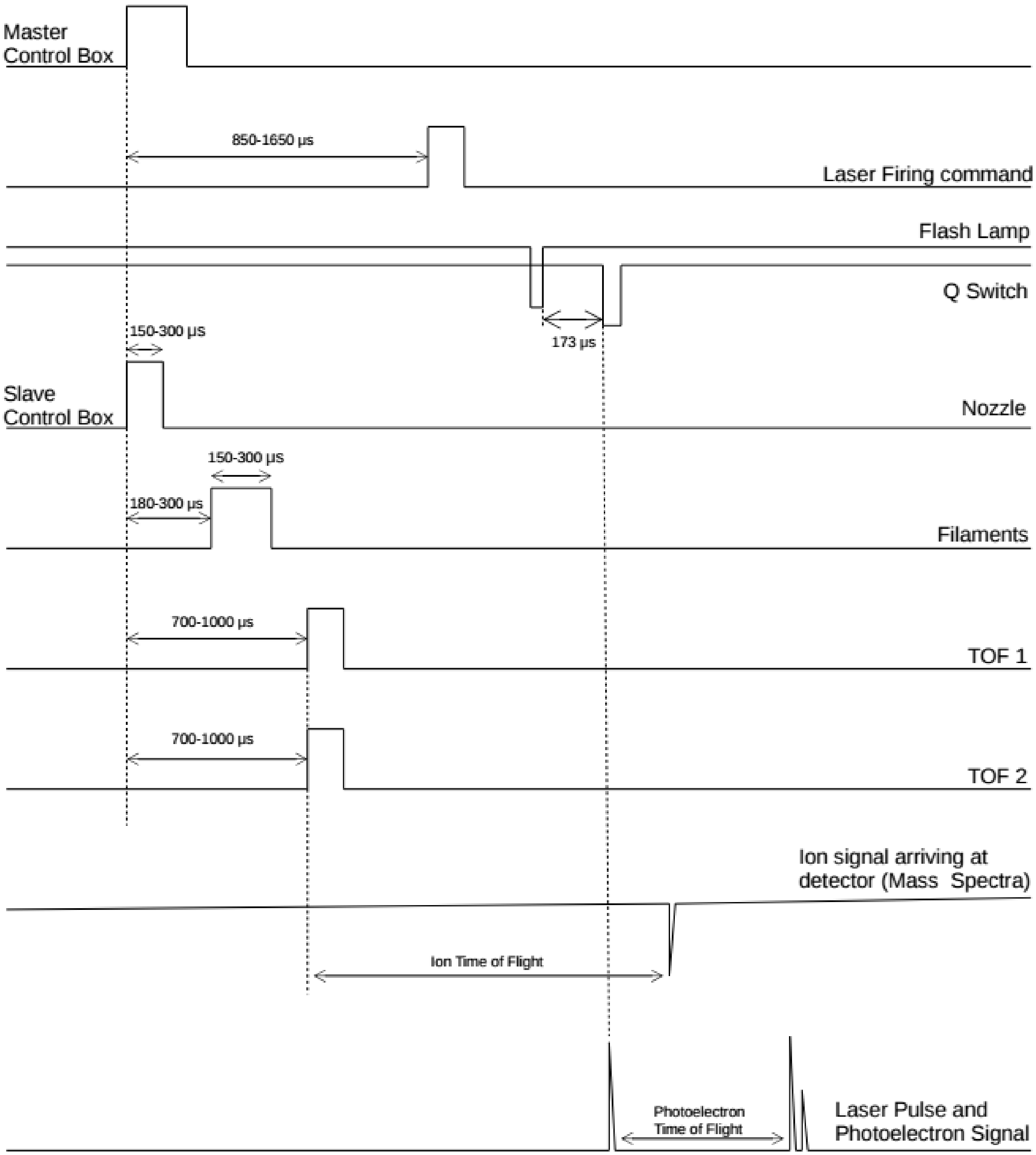

Figure B.1: Schematic displaying the timing of the various TOF-PES components.